HHS Public Access

Author manuscript

Biochemistry. Author manuscript; available in PMC 2020 February 12.

Published in final edited form as:

Biochemistry. 2019 February 12; 58(6): 833–847. doi:10.1021/acs.biochem.8b01153.

Kinetic Analyses of the Siderophore Biosynthesis Inhibitor Salicyl-AMS and Analogues as MbtA Inhibitors and Antimycobacterial Agents

Glennon V. Bythrow[†,§], **Poornima Mohandas**[†,§], **Tezcan Guney**[^], **Lisa C. Standke**[#], **Gabrielle A. Germain**[†,§], **Xuequan Lu**[^], **Cheng Ji**[^], **Keith Levendosky**[†,§], **Sivagami Sundaram Chavadi**[†], **Derek S. Tan**[*,#,¥], and **Luis E. N. Quadri**[*,†,§,‡]

[†]Department of Biology, Brooklyn College, City University of New York, 2900 Bedford Avenue, Brooklyn, New York 11210, United States

[§]Biology Program, Graduate Center, City University of New York, 365 Fifth Avenue, New York, New York 10016, United States

[^]Chemical Biology Program, Sloan Kettering Institute, Memorial Sloan Kettering Cancer Center, 1275 York Ave., New York, New York 10065, United States

[#]Pharmacology Program, Weill Cornell Graduate School of Medical Sciences, Memorial Sloan Kettering Cancer Center, 1275 York Ave., New York, New York 10065, United States

[¥]Tri-Institutional Research Program, Memorial Sloan Kettering Cancer Center, 1275 York Ave., New York, New York 10065, United States

[‡]Biochemistry Program, Graduate Center, City University of New York, 365 Fifth Avenue, New York, New York 10016, United States, United States

Abstract

There is a paramount need for expanding the drug armamentarium to counter the growing problem of drug-resistant tuberculosis. Salicyl-AMS, an inhibitor of salicylic acid adenylation enzymes, is a first-in-class antibacterial lead compound for the development of tuberculosis drugs targeting the biosynthesis of salicylic acid-derived siderophores. In this study, we determined the K_i of salicyl-AMS for inhibition of the salicylic acid adenylation enzyme MbtA from *Mycobacterium tuberculosis* ($MbtA_{tb}$), designed and synthesized two new salicyl-AMS analogues to probe structure–activity relationships (SAR), and characterized these two analogues alongside salicyl-

[*]**Corresponding Authors:** L.E.N.Q.: Biology Department, Brooklyn College, City University of New York, Brooklyn, New York 11210-2850; LQuadri@brooklyn.cuny.edu. D.S.T.: Sloan Kettering Institute, Memorial Sloan Kettering Cancer Center, New York, New York 10065-6007; tand@MSKCC.ORG.

ASSOCIATED CONTENT

Supporting Information

The following files are available free of charge.

Supplemental materials and methods, figures, and tables (PDF)

Accession Codes

MbtA: UniProtKB P71716

Notes

The authors declare competing financial interest. D.S.T. and L.E.N.Q. are inventors on U.S. Patents 8,461,128 and 8,946,188. D.S.T., L.E.N.Q, L.C.S., and G.V.B. are inventors on a patent application based on this work.

AMS and six previously reported analogues in biochemical and cell-based studies. The biochemical studies included determination of kinetic parameters $\left(K_i^{app}, k_{on}^{app}, K_{off}, \text{ and } t_R\right)$ and analysis of the mechanism of inhibition. For these studies, we optimized production and purification of recombinant $MbtA_{tb}$, for which K_m and k_{cat} values were determined, and used the enzyme in conjunction with an $MbtA_{tb}$-optimized, continuous, spectrophotometric assay for MbtA activity and inhibition. The cell-based studies provided an assessment of the antimycobacterial activity and post-antibiotic effect of the nine $MbtA_{tb}$ inhibitors. The antimycobacterial properties were evaluated using a strain of non-pathogenic, fast-growing *Mycobacterium smegmatis* that was genetically engineered for $MbtA_{tb}$-dependent susceptibility to inhibitors. This convenient model system greatly facilitated the cell-based studies by bypassing the methodological complexities associated with the use of pathogenic, slow-growing *M. tuberculosis.* Collectively, these studies provide new information on the mechanism of inhibition of $MbtA_{tb}$ by salicyl-AMS and eight analogues, afford new SAR insights for these inhibitors, and highlight several suitable candidates for future preclinical evaluation.

Graphical Abstract

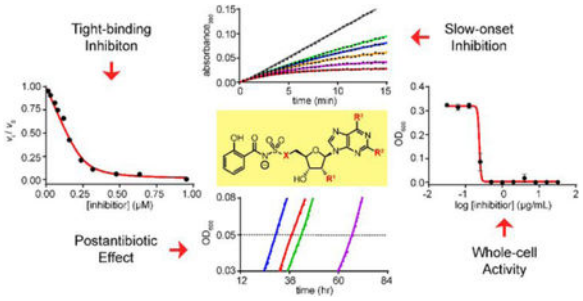

INTRODUCTION

Mycobacterium tuberculosis (*Mtb*), the causative agent of tuberculosis, is a resilient, obligate bacterial pathogen with a devastating impact on global public health.[1] The intrinsic clinical resistance of *Mtb* to many antimicrobial drugs is one of the challenges at the center of the problematic chemotherapy and global control of tuberculosis.[2] Standard tuberculosis treatment requires prolonged and expensive chemotherapy with multiple drugs, and is associated with adverse side effects and compliance challenges.[3,4] The cumbersome chemotherapy regimens against tuberculosis result in high frequency of suboptimal or incomplete drug treatment courses,[4,5] a situation that over the decades has led to the rise of tuberculosis cases produced by multidrug-resistant (MDR) and extensively drug-resistant (XDR) strains of *Mtb*.[1] The rise of these resistant strains compounds the already challenging problem of tuberculosis chemotherapy and presents a growing threat to global tuberculosis control and eradication efforts. This grim scenario underscores the need for expanding the antituberculosis drug armamentarium.

Towards this end, we previously developed the first-in-class nucleoside antibiotic salicyl-AMS (5′-*O*-[*N*-salicylsulfamoyl]adenosine) (**1**, Figure 1A).[6] We rationally-designed **1** as a salicyl-AMP intermediate mimetic inhibitor of the enzyme MbtA of *Mtb* ($MbtA_{tb}$, Figure

1B).[7] MbtA has no human homologues and is required for the biosynthesis of salicylic acid-derived mycobactin (MBT) siderophores, which are high-affinity Fe^{3+} chelators involved in the scavenging and uptake of iron (Fe),[7,8] a micronutrient essential for *Mtb* growth and pathogenesis (Figure 1C).[9–11] The realization of the critical role of the MBT siderophore system in *Mtb* biology emerges from multiple studies demonstrating that *Mtb* mutant strains with gene knockouts in the siderophore biosynthesis or transport systems have impaired survival in macrophages[12–14] and various degrees of attenuation in guinea pig[14] and mouse[13,15–17] models of tuberculosis. Thus, MBT biosynthesis is considered an attractive potential target for developing tuberculosis drugs with novel mechanisms of action.[18–20]

Our previous *in vitro* studies on salicyl-AMS (**1**) demonstrated that it is a potent, selective, tight-binding inhibitor (TBI) of $MbtA_{tb}$, as well as other salicylate adenylation enzymes from pathogenic bacteria,[6] including YbtE from *Yersinia pestis*[21] and PchD from *Pseudomonas aeruginosa*.[22] Moreover, we have shown that salicyl-AMS (**1**) inhibits the biosynthesis of MBTs in *Mtb* and, as expected, restricts the growth of the pathogen with much greater potency under Fe-limiting conditions,[6] in which production of MBTs is crucial for Fe acquisition. In all, this early work provided proof of principle for the druggability of salicylate adenylation enzymes, validated pharmacological inhibition of siderophore biosynthesis as a new mechanism of antibiotic action, and established salicyl-AMS (**1**) as a first-in-class antibacterial lead compound for the development of tuberculosis drugs targeting siderophore biosynthesis. Subsequent studies by Aldrich and coworkers confirmed the inhibitory activity of salicyl-AMS (**1**) against $MbtA_{tb}$ and *Mtb*, demonstrated that the inhibitor is not cytotoxic against mammalian cells, and provided extensive *in vitro* structure–activity relationship (SAR) analysis for inhibition of $MbtA_{tb}$ biochemical activity and *Mtb* growth using a wide range of salicyl-AMS analogues.[23–32]

More recently, we have also reported studies on the *in vivo* efficacy of salicyl-AMS (**1**) in a mouse model of tuberculosis.[33] Importantly, this work showed that monotherapy with salicyl-AMS (**1**) at 5.6 or 16.7 mg/kg correlated with a significant reduction of *Mtb* growth in the mouse lung, thus supporting $MbtA_{tb}$ as a promising target for the development of novel tuberculosis drugs blocking siderophore biosynthesis. However, we also observed *in vivo* toxicity at ≥16.7 mg/kg doses, precluding further dose escalation to improve efficacy. Thus, there is a continued need to develop new salicyl-AMS analogues with the long-term goal of improving pharmacokinetics, efficacy, and toxicity profiles.

Towards this end, we report herein detailed *in vitro* evaluation of salicyl-AMS (**1**), two novel salicyl-AMS analogues designed to probe new SAR regions, and six of the most potent analogues reported previously by Aldrich and coworkers.[28] We determined intrinsic K_i values for salicyl-AMS (**1**), biochemical residence times and other kinetic parameters of these tight-binding inhibitors, and assessed them for antibacterial and post-antibiotic effects in cell culture. In the course of this work, we also optimized production and purification of recombinant $MbtA_{tb}$ and developed new cellular models using the non-pathogenic, fast-growing *Mycobacterium smegmatis* (*Msm*) species. Collectively, these studies provide new information on the mechanism of inhibition of $MbtA_{tb}$ by salicyl-AMS (**1**) and eight analogues, provide new SAR insights for $MbtA_{tb}$ inhibitors, and highlight several $MbtA_{tb}$ inhibitors as suitable candidates for further preclinical evaluation.

MATERIALS AND METHODS

Synthesis of MbtA inhibitors.

Salicyl-AMS (**1**)[6] was synthesized by WuXi AppTec (Shanghai, China). Salicyl-2′-dAMS (**2**),[25] salicyl-2-Ph-AMS (**3**),[23] salicyl-2-PhNH-AMS (**4**),[23] salicyl-AMSN (**4a**),[24] salicyl-6-*N*-Me-AMS (**5a**),[23] and salicyl-6-*N*-*c*-Pr-AMS (**5b**),[23] were synthesized as previously described. Salicyl-AMSNMe (**4b**) was synthesized in seven steps from 6-*N*-Boc-2′,3′-isopropylideneadenosine (Figure S1). Salicyl-6-MeO-AMSN (**6**) was synthesized in 10 steps from inosine (Figure S2). Compounds (except **6**) were converted to the corresponding sodium salts by ion exchange (see Supporting Information).

Overexpression and purification of $H_{10}MbtA^{opt}$.

Mtb MbtA (UniProtKB P71716), codon-optimized for expression in *Escherichia coli* with an *N*-terminal His_{10} tag ($H_{10}MbtA^{opt}$), was overproduced in *E. coli* BL21(DE3)pLysS carrying plasmid $pH_{10}MbtA^{opt}$ (see Supporting Information for codon optimization and Tables S1 and S2 for strains and plasmids used in this study, respectively). The strain was cultured in Luria-Bertani broth[34] in Fernsbach baffled flasks (wide-mouth, 2.8-L capacity) under rotary agitation (220 rpm) at 25 °C to OD_{600} = 0.3. The temperature was then reduced to 20 °C and incubation was continued. Protein overproduction was induced by addition of 1 mM IPTG (isopropyl β-d-1-thiogalactopyranoside) at $OD_{600} \approx 0.6$. After 16 h of additional incubation, the cultures were chilled on ice and the cells were harvested by centrifugation. The cells were resuspended in 20 mL of lysis buffer per liter of culture (50 mM Tris·HCl, pH 8; 10 mM imidazole; 0.5 M NaCl; 20% sucrose; 1 mM -mercaptoethanol; 1 mM PMSF; 0.1% IGEPAL CA-630). Lysozyme (300 μg/ml), DNase I (100 μg/ml), and $MgCl_2$ (25 mM) were added to the cell suspension, which was then incubated at 0 °C for 30 min and subsequently subjected to a freeze/thaw cycle for lysis. The lysate was then sonicated (Branson Ultrasonics Digital Sonifier; 2 × 30 sec, 90% intensity), diluted 1.3 times in lysis buffer, subjected to high-speed centrifugation (1 h, 20,000 g), filtered (Whatman filter paper, 2.7 μm pore size), and degassed under reduced pressure. $H_{10}MbtA^{opt}$ was purified from the cleared lysate by Ni^{2+}-column chromatography using Ni–NTA Superflow resin according to the manufacturer's instructions (Qiagen) and an ÄKTA Purifier UPC10 FPLC System (GE Healthcare). The loaded column (7 mL) was washed with 5 column volumes of wash buffer (75 mM Tris·HCl, pH 8; 20 mM imidazole; 0.5 M NaCl; 5% glycerol), and proteins were eluted using an imidazole gradient [solvent A: wash buffer; solvent B: elution buffer (75 mM Tris·HCl, pH 8; 0.8 M imidazole; 0.2 M NaCl; 5% glycerol)]. $H_{10}MbtA^{opt}$ eluted at ≈0.36 M imidazole. Fractions containing $H_{10}MbtA^{opt}$ were then dialyzed (Slide-A-Lyzer Dialysis cassettes; Pierce) into dialysis buffer (25 mM Tris·HCl, pH 8; 0.2 M NaCl; 2 mM DTT; 5% glycerol), aliquoted, flash-frozen, and stored at –80 °C. Protein fraction quality and protein concentration were determined by SDS-PAGE (sodium dodecyl sulfate polyacrylamide gel electrophoresis) analysis[34] and Bio-Rad Protein Assay (Bio-Rad Laboratories, Inc.), respectively.

Assay for $MbtA_{tb}$ activity and inhibition.

The adenylation activity of $H_{10}MbtA^{opt}$ and its inhibition were evaluated using a $H_{10}MbtA^{opt}$-optimized version of the hydroxylamine–7-methyl-6-thioguanosine (HA–

MesG) continuous, spectrophotometric assay.[35] The assay was carried out in a 96-well plate format as we have recently reported.[36] The assay reaction mixture was optimized for $H_{10}MbtA^{opt}$ activity. Optimization experiments included evaluation of various concentrations of Tris·HCl (and pH), hydroxylamine, MesG, ATP, NaCl, $MgCl_2$, glycerol, reducing agents (DTT and TCEP), and detergent [IGEPAL CA-630, Triton-X100, and CHAPS (3-[(3-cholamidopropyl)dimethylammonio]-1-propanesulfonate)]. Unless otherwise indicated for specific experiments, the optimized assay reaction mixture contained the following: 50 mM Tris·HCl, pH 8.0; 3 mM $MgCl_2$; 0.5 mM DTT; 0.1 U purine nucleoside phosphorylase (PNP); 0.04 U inorganic pyrophosphatase (PPT); 450 mM hydroxylamine; 0.4 mM MesG; 1 mM ATP; 300 μM salicylic acid; 0.01% CHAPS buffer; 7.5% ultrapure glycerol; and $H_{10}MbtA^{opt}$ at concentrations noted for specific experiments. When needed, MbtA inhibitors were added from 10% DMSO stock solutions, with a final DMSO concentration of 1% in both inhibitor-containing reactions and control reactions (no inhibitor). Reactions were preincubated for 10 min at 25 °C before being initiated by the addition of either salicylic acid for steady state kinetic analysis or $H_{10}MbtA^{opt}$ for progress curve analysis. The phosphorolysis of MesG was measured continuously at either regular 1-min intervals (for steady state kinetic analysis) or 25-sec intervals (for progress curve analysis) for up to 45 min, at 360 nm and 25°C in a DTX 880 multimode detector microplate reader (Beckman Coulter, Inc.). The concentration of active $H_{10}MbtA^{opt}$ was validated by active-site titration[37] using salicyl-AMS (**1**) as the reference inhibitor. The calculated concentration of total $H_{10}MbtA^{opt}$ used in the assays was essentially indistinguishable from the concentration of active $H_{10}MbtA^{opt}$ determined by active-site titration (not shown).

Determination of K_m and k_{cat}.

Experiments to determine the K_m value for ATP $\left(K_m^{ATP}\right)$ were carried out with ATP in the 1–67.5 μM range (1.5-fold dilution series) and a saturating salicylic acid concentration of 300 μM. Experiments to determine the K_m value for salicylic acid $\left(K_m^{sal}\right)$ were done with salicylic acid in the 0.027–1.3 μM range (1.5-fold dilution series) and a saturating ATP concentration of 1 mM. $H_{10}MbtA^{opt}$ and $MgCl_2$ were used at 250 nM and 5 mM, respectively. The spectrophotometric data were analyzed to calculate initial velocity (v_0) data. K_m and k_{cat} values were then determined by nonlinear regression analysis of background-corrected v_0 versus substrate concentration ([S]) datasets using the Henri–Michaelis–Menten equation with V_{max} replaced by enzyme concentration ([E]) × k_{cat}[38] (Eq. 1). Prism v6.01 (GraphPad Software, Inc.) was used for curve-fitting, regression analyses, and statistical analyses of these datasets and all other experimental datasets generated in this study. The K_m and k_{cat} values reported are averages of two independent experiments.

$$v_0 = \frac{[S][E]k_{cat}}{[S] + K_m} \quad \text{Eq. 1}$$

Determination of K_i.

The K_i of salicyl-AMS (**1**) for $H_{10}MbtA^{opt}$ was determined by Morrison analysis for TBIs.[37,39] Two K_i values were determined using two experimental modalities with respect to substrates. One modality used variable, saturating concentrations of ATP (0.86–6.5 mM range) along with a constant, saturating concentration of salicylic acid (300 μM). The other modality used variable, saturating concentrations of salicylic acid (30.6–310 μM range) along with a constant, saturating concentration of ATP (6.5 mM). $H_{10}MbtA^{opt}$ and $MgCl_2$ were used in the assays at 250 nM and 15 mM, respectively. Salicyl-AMS (**1**) was tested using a 50–1,040 nM range. The range was covered using a 2-fold dilution series format for sections A and C of the dose-response curve and a 1.2-fold dilution series format for section B ("elbow") of the curve as recommended.[37,40] The spectrophotometric data were used to determine fractional initial velocities (v_i/v_0), where v_i is the initial velocity with inhibitor and v_0 is the initial velocity with no inhibitor (DMSO controls). K_i^{app} values were calculated by Morrison analysis of background-corrected v_i/v_0 versus logarithm of inhibitor concentration ([I]) datasets using Eq. 2, as described[37]. A K_i value was then obtained from each of the two datasets of K_i^{app} values vs. [S] as the *y*-intercept of the linear regression of the data fitted to Eq. 3.[39] Each of the two K_i values reported was calculated from the average of K_i^{app} datasets generated from three independent experiments.

$$\frac{v_i}{v_0} = 1 - \frac{\left([E] + [I] + K_i^{app}\right) - \sqrt{\left([E] + [I] + K_i^{app}\right)^2 - 4[E][I]}}{2[E]} \quad \text{Eq. 2}$$

$$K_i^{app} = K_i\left(1 + \frac{[S]}{K_m}\right) \quad \text{Eq. 3}$$

Progress curves and determination of kinetic parameters K_i^{app}, k_{on}^{app}, k_{off}, and t_R.

Reactions were pre-incubated for 10 min before being initiated by the addition of $H_{10}MbtA^{opt}$ (1 μM). The concentration range at which each inhibitor was tested was selected empirically by pilot experiments (not shown). The ranges were as follows: 4,000–1,041 nM range (1.4-fold dilution series) for **1**, **4a**, **4b**, **5a**, **5b**, and **6**; 2,000–1,157 nM range (1.2- and 1.3-fold dilution series combination) for **3a**; 3,000–1,366 nM range (1.3- and 1.5-fold dilution series combination) for **3b**; and 2,857–1,041 nM range (2.2- and 1.4-fold dilution series combination) for **2**. As done in similar studies,[41,42] the background-corrected spectrophotometric data were fitted to Eq. 4.[43] In Eq. 4, A is the absorbance at time t, v_{ps} is the pre-steady state initial velocity, v_s is the steady-state velocity at equilibrium, and k_{obs} is the rate constant for progression to steady state. The datasets of v_s versus [I] derived from the progress curves were fitted to Eq. 2 to calculate the K_i^{app} values. The k_{obs} values were determined with Eq. 4 for each inhibitor concentration and then used to calculate the

dissociation rate constant (k_{off}) values using Eq. 5,[44] as previously reported.[45,46] Subsequently, k_{on}^{app} values were determined using Eq. 6 and the calculated k_{off} and the K_i^{app} values.[44] Residence time (t_R) values were calculated as the reciprocal of the k_{off} value. To assess the inhibition mechanisms of the inhibitors, k_{obs} values versus [I] datasets were plotted and fitted to Eq. 7.[44] Each kinetic parameter reported is the average derived from a minimum of five independent experiments. Pearson correlation analysis between kinetic parameters was carried out using the statistical analysis package in Prism v6.01. Pearson correlation coefficients (PCCs) with Student's *t*-test *p* values ≤0.05 were considered statistically significant.

$$A = v_s t + \frac{v_{ps} - v_s}{k_{obs}}\left[1 - e\left(-k_{obs} t\right)\right] \quad \text{Eq. 4}$$

$$k_{off} = k_{obs}\frac{v_s}{v_{ps}} \quad \text{Eq. 5}$$

$$k_{on}^{app} = \frac{k_{off}}{K_i^{app}} \quad \text{Eq. 6}$$

$$k_{obs} = k_{on}[I] + k_{off} \quad \text{Eq. 7}$$

Bacterial culturing and recombinant DNA manipulations.

Msm mc^{2}155 (ATCC 700084)[47] and its derivatives were regularly cultured under standard conditions in Middlebrook 7H9 or 7H11 (Difco) supplemented as reported.[8] *Msm* strains were cultured in Fe-limiting GASTD medium or GASTD supplemented with 100 μM $FeCl_3$ (GASTD+Fe medium)[6,48] for specific experiments as noted below. Routine culturing of *E. coli* strains was done under standard conditions in Luria-Bertani media.[34] When required, kanamycin (30 μg/ml), chloramphenicol (34 μg/ml), ampicillin (100 μg/ml), sucrose (2%), and/or 5-bromo-4-chloro-3-indolyl-β-d-galactopyranoside (X-gal, 70 μg/ml) were added to the growth media. DNA manipulations were carried out using established protocols and *E. coli* DH5α as the primary cloning host.[34] PCR-generated DNA fragments used in plasmid constructions were sequenced to verify fidelity. The oligonucleotides used in this study are shown in Table S3. Genomic DNA isolation, plasmid electroporation into *Msm*, and selection of *Msm* transformants were carried out as reported.[8] Unless otherwise indicated, molecular biology, biochemical, and microbiology reagents were purchased from Sigma-Aldrich Inc., Thermo Fisher Scientific Inc., New England Biolabs Inc., QIAGEN Inc., or Integrated DNA Technologies Inc.

Generation of *M. smegmatis* mutants ΔE, ΔEM, and ΔEM-pMbtA$_{tb}$.

Mutants were generated using the p2NIL/pGOAL19-based flexible cassette method,[49] as reported.[8] *Msm* ΔE carried an unmarked, in-frame deletion of *MSMEG_0019*, encoding the peptide synthetase (7,523 amino acids, the largest protein in *Msm*[50]) predicted to be essential for biosynthesis of exochelin (EXO) siderophores.[51–53] A *MSMEG_0019* deletion cassette-delivery, suicide plasmid (pΔ0019) was used to generate the chromosomal deletion, which eliminated codons 5 through 7,519 of the gene. The deletion cassette contained from 5′- to 3′-end: the 984-bp segment upstream of the gene, the gene's first 4 codons, the gene's last 4 codons, the stop codon, and the 1,029-bp segment downstream of the gene. To generate the cassette, primer pair OF0019 and IR0019soe and primer pair IF0019soe and OR0019 were first used to generate the 5' fragment (1,011 bp) and the 3' fragment (1,059 bp) for the cassette, respectively, from genomic DNA template. The fragments, which had a 30-bp overlap at the splice site embedded in IF0019soe and IR0019soe, were then used together as a template for PCR with primers OF0019 and OR0019 to fuse the fragments. The PCR-generated cassette was cloned into pCR2.1Topo (TOPO TA Cloning Kit, Invitrogen, Thermo Fisher Scientific Inc.), then excised from the pCR2.1Topo construct using HindIII and EcoRV, and religated into p2NIL[49] linearized by HindIII-PmlI digestion. The resulting plasmid (p2NILΔ0019) and pGOAL19[49] were digested with PacI, and then the PacI marker cassette of pGOAL19 was ligated to the linearized p2NILΔ0019 to create pΔ0019. Electroporation of pΔ0019 into *Msm* wild-type (WT) and selection of potential single- and double-crossover mutants were conducted as reported.[8] The *MSMEG_0019* deletion was screened for and confirmed by PCR using two primer pairs (OF0019 and OR0019: yielding an undetectable 24,585-bp amplicon for WT and a 2,040-bp amplicon for mutant; IF0019 and IR0019: yielding a 148-bp amplicon for WT and no amplicon for mutant) (not shown).

EXO/MBT-deficient *Msm* ΔEM carried the *MSMEG_0019* deletion noted above and an unmarked, in-frame deletion of *Msm mbtA* (*mbtA*$_{sm}$), which encodes the salicylate adenylation enzyme essential for MBT biosynthesis.[8] The *mbtA*$_{sm}$ deletion left behind only the gene's start codon followed by the stop codon, and it was created in *Msm* ΔE with the same approach we have previously reported for generation of the identical *mbtA*$_{sm}$ deletion in *Msm* WT to generate the mutant referred to hereafter as *Msm* ΔM.[8]

Msm ΔEM was transformed with plasmid pMbtA$_{tb}$ (expressing *mbtA*$_{tb}$) to generate strain *Msm* ΔEM-pMbtA$_{tb}$. To construct pMbtA$_{tb}$, a DNA fragment encompassing *mbtA* of *Mtb* (*mbtA*$_{tb}$, Rv2384[8]) was generated by PCR from genomic DNA template using primer pair mbtA$_{tb}$F1 and mbtA$_{tb}$R1. The PCR product, which included an optimized ribosome-binding site[54] upstream of *mbtA*$_{tb}$ introduced by primer mbtAtbF1, was cloned into pCR2.1Topo. Subsequently, the insert was recovered from the pCR2.1Topo construct as a HpaI-NheI fragment and subcloned into the mycobacterial, low-copy number plasmid pCP0[55] linearized by HpaI-NheI digestion. This subcloning created pMbtA$_{tb}$, in which *mbtA*$_{tb}$ is under the control of the constitutive mycobacterial *hsp60* promoter located in pCP0.

Growth inhibition assays.

Dose-response experiments using microdilution assays in a 96-well plate platform were performed as reported.[48,56] *Msm* strains were grown in GASTD or GASTD+Fe media. Cultures (200 μL/well) were started at OD_{600} = 0.0005 (≈9×10^4 CFU/well, as per concurrent CFU determination) from culture stocks prepared in GASTD medium as reported.[6] Growth was assessed as OD_{600} after 4 days of incubation (37 °C, 170 rpm) using the DTX 880 microplate reader. Unless otherwise indicated in specific experiments, compounds were typically evaluated using a 0.031–64 μg/ml range (2-fold dilution series format). Inhibitors were added from 10% DMSO stock solutions, with a final DMSO concentration of 0.5% in both inhibitor-treated cultures and DMSO controls (no inhibitor). Minimum inhibitory concentration (MIC) values were calculated as the lowest concentration tested that inhibited growth by ≥95% relative to DMSO controls. Data presented are derived from three independent experiments.

Post-antibiotic effect (PAE) assays.

Cells from mid-log growth phase cultures of *Msm* ΔEM-p$MbtA_{tb}$ in GASTD medium (37 °C, 170 rpm, OD_{600} ≈ 0.75) were harvested by centrifugation and washed in GASTD medium (3 times with 1 culture volume). The washed cells were resuspended in GASTD medium and transferred to U-bottom 96-well cell culture plates (Corning, Inc.) for inhibitor exposure at a cell density corresponding to OD_{600} = 1.0 (50 μL/well). Cells were exposed to 5×, 50×, and 100× average MIC value, in line with reported studies with other antimycobacterial compounds.[57] Inhibitors were added from 10% DMSO stock solutions, with a final DMSO concentration of 1% in both inhibitor-exposed cultures and DMSO controls (no inhibitor). After the exposure period (1 h, 37 °C, 170 rpm), the cultures were diluted in pre-warmed, inhibitor-free medium to OD_{600} = 0.001 (1,000-fold dilution, bringing inhibitor concentrations to 0.005×, 0.05×, and 0.1× average MIC values) and reseeded into flat-bottom, 96-well culture plates (Corning, Inc.) at 200 μl/well. The 96-well plates were incubated for culture growth at 37 °C in a FLUOstar Optima microplate reader (BMG Labtech, Inc.), and OD_{600} readings were taken every 30 min following plate shaking (5 min, 200 rpm) for 5 days. The growth vs. time datasets were analyzed to determine the time at which cultures reached an exponential growth phase threshold of OD_{600} = 0.05 (≈15% of maximal growth). The time-to-threshold data were used to calculate PAE as the difference between the time-to-threshold values of the inhibitor-exposed culture and the control cultures.[58] Data presented are derived from three independent experiments. Pearson correlation analysis between PAE and t_R datasets was carried out using Prism v6.01, and PCCs with p values ≤0.05 were considered statistically significant.

RESULTS AND DISCUSSION

Cloning, overexpression, and purification of recombinant $MbtA_{tb}$.

$MbtA_{tb}$ catalyzes formation of the first covalent acyl-enzyme intermediate during MBT acyl-chain assembly[7] and is the molecular target of the antibacterial lead compound salicyl-AMS (**1**)[6] (Figure 1). Previous approaches for purification of recombinant $MbtA_{tb}$ expressed in *E. coli* have been characterized by low yields (0.1–2 mg/L) due to low expression, poor solubility, inefficient affinity tag removal, and/or the need for multiple purification steps.

[6,7,25] We sought to overcome this limitation and to make $MbtA_{tb}$ more readily available for our biochemical and inhibition studies. To this end, we explored codon optimization, alternative polyhistidine-tag fusion strategies, and changes in expression and purification conditions. We first carried out codon optimization, which led to changes in 322 of the 566 codons of *mbtA*$_{tb}$ (Figure S3). We then evaluated ten different polyhistidine affinity tag strategies (*viz.* alternative tag lengths and locations, double tags, and a tandem tag) for the codon-optimized $MbtA_{tb}$ ($MbtA^{opt}$) (Figure S4A). This included unconventional tags that have been shown to be advantageous with other problematic recombinant proteins.[59,60] Pilot experiments for assessment of protein expression, solubility, and binding to Ni^{2+}-charged resin revealed that *N*-terminal deca-His tagged $MbtA^{opt}$ ($H_{10}MbtA^{opt}$) had the best properties overall (not shown). Thus, we advanced $H_{10}MbtA^{opt}$ to larger-scale overproduction and purification experiments that ultimately led to the final methodology used to obtain the enzyme for the biochemical and inhibition studies described below. Overall, the optimizations and methodological improvements shortened the purification protocol by eliminating the need for tag cleavage and size exclusion chromatography, rendered purified $H_{10}MbtA^{opt}$ with purity levels comparable to those reported for other recombinant $MbtA_{tb}$ variants (Figure S4B), and permitted final yields of up to ≈8 mg/L. This represents a 4-fold increase relative to the highest yield previously reported for $MbtA_{tb}$.[25]

Validation of $H_{10}MbtA^{opt}$ activity and inhibition by salicyl-AMS in the HA–MesG kinetic assay.

$H_{10}MbtA^{opt}$ is a novel recombinant variant of $MbtA_{tb}$ with a relatively large His_{10} tag that could potentially hinder the salicylate adenylation activity of the enzyme and/or the ability of salicyl-AMS (**1**) to inhibit this activity with a potent, TBI modality.[6] Therefore, we sought to validate the activity of $H_{10}MbtA^{opt}$ and its inhibition by salicyl-AMS (**1**). We have previously used a traditional ATP–$^{32}PP_i$ isotope exchange (ATP-PP_i) assay to characterize the adenylation activity of $MbtA_{tb}$[7] and its inhibition by salicyl-AMS (**1**).[6] Although this is a robust assay, it measures the reverse of the adenylation reaction and has several methodological disadvantages, including those arising from its end-point nature, the need for radiolabeled reagents, and a poor suitability for high-throughput analysis. Thus, we explored the adoption of a more convenient spectrophotometric HA–MesG kinetic assay that measures enzyme activity in the relevant forward direction of the biosynthetic pathway and has been recently validated with several adenylation enzymes, including $MbtA_{tb}$.[35] To this end, we used our recently reported study applying the HA–MesG assay to the characterization of a TBI of the cysteine adenylation domain of the *Y. pestis* siderophore synthetase HMWP2[36] as a methodological template. Encouragingly, results of the first assessment of the activity of $H_{10}MbtA^{opt}$ and its inhibition by salicyl-AMS (**1**) using the HA–MesG assay demonstrated enzyme activity and the expected TBI behavior for **1** (*i.e.* $IC_{50} \approx ½$ [E]) (Table 1, Figure S5). Out of an abundance of caution, we assessed whether salicyl-AMS (**1**) had any inhibitory effect on the PPT-PNP coupling system of the HA–MesG assay. We also evaluated whether any of four salicyl-AMS fragments that could possibly result from hydrolytic degradation of **1** and/or be present as trace contaminants (*i.e.*: AMS (**7**), salicyl-sulfamate (**8**), salicylamide (**9**), and N^3-5′-cycloadenosine (**10**); Table S4) had a negative impact on the HA–MesG assay. We found that salicyl-AMS (**1**) did not

affect the PPT-PNP coupling system when tested at up to 40 μM (10 times the maximum concentration of **1** used in the HA–MesG assay), and only salicyl-sulfamate (**8**) depressed the $H_{10}MbtA^{opt}$-dependent signal in the HA–MesG assay, however only to a negligible extent ($IC_{50} \approx 1$ mM) (Table S4). Therefore, inhibition by an off-target effect of salicyl-AMS (**1**) or by potential trace amounts of fragments **7**–**10** is not an assay confounder.

The validation experiments noted above were carried out using the generic conditions of the HA–MesG assay originally reported.[35] Thus, we optimized the assay for $H_{10}MbtA^{opt}$ prior to its use in additional enzyme and inhibitor characterization studies. This optimization led to several changes in reaction composition and a ≈ 3-fold increase in $H_{10}MbtA^{opt}$ activity (Figure S6). In all, our results ruled out the possibility of a detrimental effect of the His_{10} tag in $H_{10}MbtA^{opt}$ and set the stage for the use of $H_{10}MbtA^{opt}$ in conjunction with the HA–MesG assay for the studies reported here. To our knowledge, this is the first example of the use of the HA–MesG assay for the evaluation of inhibitors of a salicyl-AMP ligase.

Steady-state kinetic parameters of $H_{10}MbtA^{opt}$.

Prior to carrying out additional $H_{10}MbtA^{opt}$ inhibition studies, we determined the Michaelis −Menten parameters for $H_{10}MbtA^{opt}$ using the optimized HA–MesG assay (Figure 2). Kinetic analysis with salicylic acid as the variable substrate revealed K_m^{sal} and k_{cat}^{sal} values of 0.31 ± 0.003 μM and 0.90 ± 0.06 min^{-1}, respectively. With ATP as the variable substrate, the K_m^{ATP} and k_{cat}^{sal} values obtained were 13.0 ± 1.3 uM and 1.16 ± 0.04 min^{-1}, respectively. The agreement of the two k_{cat} values indicates consistency between the two evaluation modalities with respect to substrate and highlights the reliability of the experimental approach. Notably, the average k_{cat} value of $H_{10}MbtA^{opt}$ (≈1 min^{-1}) is comparable to those of mechanistically related 2,3-dihydroxybenzoate adenylation enzymes involved in the biosynthesis of several aryl-capped siderophores,[61] namely *E. coli* EntE (≈1 min^{-1}), *Acinetobacter baumannii* BasE (≈1 min^{-1}), and, to some extent *Vibrio cholerae* VibE (0.2 min^{-1}), when using DHBA as the variable substrate in the HA–MesG assay.[35] The relatively low k_{cat} values of these ligases determined with the surrogate acyl-acceptor hydroxylamine in the HA–MesG assay might be tentatively attributed to the lack of interaction between the ligase and its phosphopantetheinylated carrier protein partner, which is thought to be needed to trigger the rotation of the *C*-terminal domain of the ligase and facilitate the acyl transfer step.[62]

This work provided K_m^{ATP} and k_{cat}^{ATP} values for $MbtA_{tb}$ working in the relevant forward direction of the biosynthetic pathway. A previous study with a different $MbtA_{tb}$ recombinant variant and HA–MesG assay conditions not optimized for $MbtA_{tb}$ found a K_m^{sal} value identical to the one reported here, but a k_{cat}^{sal} value ≈3-fold lower than the one determined by our analysis.[35] The higher k_{cat}^{sal} value found herein might be due to a more robust $MbtA_{tb}$ recombinant variant and/or our optimized assay conditions. Interestingly, the K_m values derived from our analysis indicate that $MbtA_{tb}$ has ≈40-fold higher affinity for salicylic acid than for ATP. This finding is in agreement with the 65- and 32-fold preference for salicylic acid found with $MbtA_{tb}$ and the salicylate adenylation enzyme YbtE from *Y. pestis* (45%

sequence identity with $MbtA_{tb}$) for the reverse of the adenylation reaction in the ATP-PP_i assay.[6,25] It is worth noting, however, that the K_m^{ATP} and K_m^{sal} values derived from the ATP-PP_i assay were 10–20 times larger (*i.e.*: lower substrate affinities) than those we determined with $H_{10}MbtA^{opt}$ and the optimized HA–MesG assay.

Determination of intrinsic K_i for salicyl-AMS (1) with $H_{10}MbtA^{opt}$.

The K_i value of salicyl-AMS (**1**) for inhibition of $MbtA_{tb}$ has not been reported, and thus we determined the K_i value for $H_{10}MbtA^{opt}$ inhibition using the optimized HA–MesG assay. To this end, we followed the approach we previously applied to determine the K_i value of salicyl-AMS (**1**) for inhibition of the *Y. pestis* salicylate adenylation enzyme YbtE noted above.[6] Due to the bisubstrate nature of the adenylation reaction catalyzed by $MbtA_{tb}$, two K_i values were independently calculated using two approaches with respect to the substrates. One approach had variable saturating concentrations of ATP along with a constant, saturating concentration of salicylic acid, whereas the other had the opposite relationship of constant vs. variable substrate. For both approaches, K_i^{app} values increased linearly with increasing [S] (Figure 3). This indicated a competitive inhibition mechanism for salicyl-AMS (**1**) with respect to both $MbtA_{tb}$ substrates,[39] a property found also for a carbocyclic analogue of salicyl-AMS (**1**) with $MbtA_{tb}$ in an ATP-PP_i assay-based study[25] and suggestive of an equilibrium random mechanism for the adenylation reaction catalyzed by $MbtA_{tb}$.[63] The competitive mechanism determined for salicyl-AMS (**1**) allowed for the calculation of K_i values as the *y*-intercepts of the fit lines for the K_i^{app} value vs. [S] datasets.[39] The values determined were 0.76 ± 0.43 nM for K_i^{ATP} and 1.04 ± 0.48 nM for K_i^{sal} (Figure 3). These K_i values are essentially indistinguishable from one another, demonstrating correspondence between the two evaluation approaches with respect to substrate and underlining the robustness of the methodological approach. Notably, the average K_i value of 0.9 nM found with $MbtA_{tb}$ is comparable to our previously reported K_i for the inhibition of *Y. pestis* YbtE using the ATP-PP_i assay (0.7 nM).[6] Overall, this indicates that salicyl-AMS (**1**) is a potent salicylate adenylation enzyme inhibitor with sub-nM K_i values.

Selection of salicyl-AMS analogues for further evaluation.

We selected six previously reported salicyl-AMS analogues for detailed *in vitro* analysis (Figure 4). These compounds are among the most potent analogues reported by Aldrich and coworkers, and represent modifications in different regions of the lead compound, including deletion of the ribose 2′-hydroxyl group (salicyl-2′-dAMS, **2**),[25] replacement of the ribose 5′-oxygen (salicyl-AMSN, **4a**),[24] and substitutions of the adenine ring at the C2 position (salicyl-2-Ph-AMS, **3a**; salicyl-2-NHPh-AMS, **3b**) and 6-amino group (salicyl-6-*N*-Me-AMS, **5a**; salicyl-6-*N*-*c*-Pr-AMS, **5b**).[23]

We also designed two analogues to expand the SAR analysis (Figure 4). Salicylate adenylation enzymes are members of the ANL family (acyl-CoA synthetase, non-ribosomal peptide synthetase adenylation domain, luciferase)[62] that bind their substrates in an unusual *cisoid* conformation (Figure 5a).[64,65] In an effort to promote this pharmacophoric conformation, we introduced a 5′-*N*-methyl substituent in salicyl-AMSN as a turn element

in salicyl-AMSNMe (**4b**). The compound was synthesized by sulfamoylation and salicylation of a protected 5′-methylamino-5′-deoxyadenosine (see Supporting Information Figure S1 for complete details).

In addition, we were intrigued by reports that small 6-amino substituents could be accommodated in salicyl-AMS analogues (**5a**, **5b**).[23,66,67] In contrast, however, the corresponding inosine analogue (**11**, Figure 5b) was a poor $MbtA_{tb}$ inhibitor and exhibited no antimicrobial activity (K_i^{app} = 800nM; *Mtb* MIC > 100 μM).[23] As inosine adopts a tautomeric (6-oxo) form compared to adenine, it was proposed that a hydrogen-bond donor is required at the C6-substituent position, which could interact with the main-chain carbonyl oxygen of $MbtA_{tb}$ V352.[67,68] This was further supported by the finding that the adenine 6-*N*,*N*-dimethyl analogue (**12**) was also a weak inhibitor (K_i^{app} = 380nM; *Mtb* MIC = 50 μM).

However, the inosine tautomeric form also introduces a proton at N1 in analogue **11** and the 6-*N*,*N*-dimethyl modification introduces additional steric constraints in analogue **12**. Thus, to probe this SAR further, we introduced a 6-methoxy substituent in salicyl-6-MeO-AMSN (**6**), which lacks the C6-substituent hydrogen-bond donor but also maintains the adenine tautomeric form (N1 lone pair) and is isosteric to the active 6-*N*-methyl analogue **5a**. Notably, initial attempts to synthesize the corresponding sulfamate analogue, salicyl-6-MeO-AMS (not shown), were thwarted by product instability, necessitating replacement with the more stable sulfamide in **6**.[24] Thus, salicyl-6-MeO-AMSN (**6**) was synthesized from inosine by conversion of the 6-oxo group to a 6-methoxy group, followed by installation of the 5′-amino group, sulfamoylation, and salicylation (see Supporting Information Figure S2 for complete details).

Progress curve analysis of kinetics of $MbtA_{tb}$ inhibition by salicyl-AMS and analogues.

To evaluate the activity of the new analogues salicyl-AMSNMe (**4b**) and salicyl-6-MeO-AMSN (**6**), and to gain additional insight into the inhibition of $MbtA_{tb}$ by salicyl-AMS (**1**) and the six previously reported analogues (**2**, **3a**, **3b**, **4a**, **5a**, **5b**), we investigated the time dependence of the onset of $H_{10}MbtA^{opt}$ inhibition by each of the compounds. To this end, we determined and compared the kinetics of their $H_{10}MbtA^{opt}$ inhibition by progress curve analysis. For each compound in the series, the progress curves displayed a nonlinear profile of $H_{10}MbtA^{opt}$ inhibition with the characteristic three phases of a time-dependent, slow-onset mechanism of inhibition (Figure 6A and Figure S7A); *i.e.*: an initial linear phase that extrapolates to a slope corresponding to a pre-equilibrium initial velocity (v_{ps}) at $t = 0$; a final linear phase with a slope representing the equilibrium, steady-state velocity (v_s); and an exponential phase that connects the two linear phases with a pseudo-first order rate constant (k_{obs}) for the approach to the steady state.[43,44] In contrast, the progress curves for uninhibited reactions (DMSO controls) showed the expected linear profile of the steady-state kinetics (Figure 6A and Figure S7A). Thus, our results demonstrate that salicyl-AMS (**1**) and the eight analogues are slow-onset inhibitors of $H_{10}MbtA^{opt}$. Encouragingly, the results also provide the first indication of the potent activity of salicyl-AMSNMe (**4b**) and salicyl-6-MeO-AMSN (**6**) against $MbtA_{tb}$.

To explore further the mechanism of $MbtA_{tb}$ inhibition, progress curves were fitted to Eq. 4 for slow-onset inhibitors, and v_{ps}, v_s, and k_{obs} values were obtained for each inhibitor concentration using nonlinear regression analysis (Figure 6A and Figure S7A).[43,44] The v_{ps}, v_s, and k_{obs} values of each progress curve were then used to calculate the dissociation rate constant (k_{off}) values using Eq. 5.[44,45] Analysis of the relationship between k_{obs} values and inhibitor concentration revealed a linear trend (Figure 6B and Figure S7B), which is a property indicative of a static, slow-onset mechanism of inhibition.[44] To our knowledge, these results provide the first indication that salicyl-AMS (**1**) exhibits this type of mechanism of inhibition with its salicylate adenylation enzyme target. Moreover, our analysis demonstrates that all of the analogues also exhibited this mechanism of inhibition. Incidentally, salicyl-AMS (**1**) was recently shown to have a static, slow-onset inhibitory mechanism with the 2,3-dihydroxybenzoate adenylation enzyme EntE from *E. coli* (40% sequence identity with $MbtA_{tb}$) in a study using a methodology not reliant on the HA–MesG assay[41]. This reinforces our overall conclusions as to the inhibitory mechanism of salicyl-AMS (**1**) with its $MbtA_{tb}$ target and supports our methodological approach, thus increasing the confidence in the inhibitory mechanism assignment made for the eight salicyl-AMS analogues analyzed.

Determination of kinetic parameters for inhibition of $H_{10}MbtA^{opt}$ by salicyl-AMS and analogues.

To characterize further the kinetic underpinnings of the inhibition of $MbtA_{tb}$ by salicyl-AMS (**1**) and analogues (**2**–**6**), and to provide the first side-by-side comparison of these inhibitors, we sought to determine their K_i^{app}, k_{on}^{app}, k_{off}, and t_R kinetic parameters. Since none of the eight salicyl-AMS analogues had been previously evaluated using the HA–MesG assay, we first assessed whether any of them had an off-target effect on the PPT-PNP coupling system of the assay. We found that none of the analogues inhibited the coupling system when tested at up to ten times the maximum concentration used in the HA–MesG assay (Table S4), thus clearing the way for their evaluation with this assay. We then carried out pilot experiments to assess whether the TBI behavior of the previously reported analogues (**2**, **3a**, **3b**, **4a**, **5a**, **5b**) as per the ATP-PP_i assay[23–26] was recapitulated under the conditions of the HA–MesG assay and whether the novel analogues salicyl-AMSNMe (**4b**) and salicyl-6-MeO-AMSN (**6**) were also TBIs. Encouragingly, all inhibitors displayed IC_{50} values ≈ ½ [E], thus indicating a TBI behavior (Table 1 and Figure S5). Kinetic parameters for each of the inhibitors were then derived from analysis of progress curve datasets using established methodologies.[41,42] The results of this analysis are summarized in Table 1.

The analysis rendered K_i^{app} values in the 27–295 nM range (≈11-fold relative spread), thus indicating that all the inhibitors have potent activity against $H_{10}MbtA^{opt}$. As expected for TBIs,[37] the K_i^{app} values had a better discrimination power of inhibitory potency than the IC_{50} values, which covered a narrower 117–289 nM range (≈2.5-fold relative spread). The k_{on}^{app} values spanned a 0.00004–0.00066 $nM^{-1}min^{-1}$ range (≈17-fold relative spread), whereas the k_{off} values and the t_R values covered a 0.007–0.031 min^{-1} range and a 54–157 min range, respectively (4-fold and 3-fold relative spread, respectively). Collectively, these results

indicate that the members of the inhibitor series are relatively similar to one another in terms of their kinetic parameters. In other words, none of the structural features of the analogues setting them apart from salicyl-AMS (**1**) had a drastic impact (*i.e.*: 50-fold change) on any kinetic parameter. Encouragingly, Pearson pairwise correlation analysis revealed the somewhat expected relatively strong correlations between IC_{50} and K_i^{app} values [Pearson correlation coefficient (PCC) = 0.86, p value = 0.003] and between k_{off} and t_R values (PCC = −0.79, p value = 0.012). The correlation analysis also showed a weaker but statistically significant correlation between K_i^{app} and k_{on}^{app} values (PCC = −0.69, p value = 0.040).

A two-dimensional kinetic map representation of the kinetic parameters illustrated several SAR trends and inhibitor clustering patterns (Figure 7). We found that the K_i^{app} of salicyl-AMS (**1**) (27 nM) was the lowest in the series and that the inhibitor had the best t_R (157 min). This is perhaps not surprising considering that salicyl-AMS (**1**) has the most similar structure in the inhibitor series to that of the cognate salicyl-AMP reaction intermediate (Figure 1), which is thought to be retained tightly bound to the active site in the enzyme.[6] The loss of the ribose 2′-hydroxyl in salicyl-2′-dAMS (**2**) was well tolerated across the board, leading to a very modest worsening of the kinetic parameters relative to salicyl-AMS (**1**) (*ca.* ≤2-fold change). In agreement with this, salicyl-2′-dAMS (**2**) has been reported to exhibit a marginal potency increase relative to salicyl-AMS (**1**) (0.5-fold decrease in K_i^{app}) using the ATP-PP_i assay.[25] The three analogues with modifications at the C6-substituent of the adenine ring (**5a**, **5b**, **6**) clustered with respect to t_R and k_{off}, showing a ≈0.5-fold decrease and ≈2-fold increase, respectively, compared with salicyl-AMS (**1**). Within this triad, the pair with the native sulfamate-based linker and substitutions on the adenine 6-amino group (**5a**, **5b**) were also essentially indistinguishable from each other with respect to K_i^{app} and k_{on}^{app} values, which were in turn ≈5.5-fold higher and ≈2.5-fold lower, respectively, than those of salicyl-AMS (**1**). In contrast, replacement of the 6-amino group with a 6-methoxy group in salicyl-6-MeO-AMSN (**6**) led to a more drastic worsening of K_i^{app} and k_{on}^{app} values, which were 10-fold higher and 6-fold lower, respectively, than those of salicyl-AMS (**1**). However, this may be the result of a dominant negative effect arising from concurrent replacement of the sulfamate linker of salicyl-AMS (**1**) with a sulfamide in this analogue. Indeed, the presence of the sulfamide linker in analogues **4a**, **4b**, and **6** correlated with the worst K_i^{app} and k_{on}^{app} values in the series. This correlation contrasts with an earlier study reporting essentially indistinguishable K_i^{app} values for salicyl-AMSN (**4a**) and salicyl-AMS (**1**) as determined using the ATP-PP_i assay.[26] This difference may be due to the different experimental conditions used in the studies (*i.e.*: different assay, recombinant proteins, batches of inhibitors, etc.). Notably, the comparison of the K_i^{app} values of salicyl-AMSN (**4a**) and salicyl-AMSNMe (**4b**) indicated that addition of the 5′-*N*-methyl substituent led to a modest 0.5-fold improvement in K_i^{app} value. This suggests that substitution of the sulfamide linker might be a strategy to mitigate the negative effect of this linker on $MbtA_{tb}$ inhibitory potency revealed by our analysis herein. Lastly, the two

analogues with aryl substituents at the adenine C2 position (**3a, 3b**) clustered away from the analogues with modifications on the adenine C6 substituent (**5a**, **5b**, **6**) and displayed the worst k_{off} and t_R values in the series. Thus, although these analogues exhibited a modest decrease (**3b**) or no decrease (**3a**) in K_i^{app} values and an increase in k_{on}^{app} values compared to salicyl-AMS (**1**), fast k_{off} rates are typically viewed as an undesired property.[69,70] It is tempting to speculate that the bulky substituents in analogues **3a** and **3b** compromise some of the binding interactions in the $MbtA_{tb}$ active site, perhaps facilitating analogue dissociation and reducing the lifetime of the analogue-$MbtA_{tb}$ complexes. Interestingly, salicyl-6-MeO-AMSN (**6**) remains a fairly potent inhibitor of $MbtA_{tb}$, despite the lack of a hydrogen-bond donor on the C6-substituent and the presence of the sulfamide linker. This result was unexpected based on previous SAR studies,[23] and is not readily rationalized based on protein structure analysis.[64,67] Nonetheless, it opens the door to further investigation of such C6-substituents.

Contrasting with our results, a previous study reported analogues **3a**, **3b**, **5a**, and **5b** to be ≈4– 24-fold more potent than salicyl-AMS (**1**) as per K_i^{app} values determined using the ATP-PP_i assay.[23] It appears that this study referenced a K_i^{app} value for salicyl-AMS (**1**) that was determined separately,[23] and this may explain the overall discrepancy with the findings reported herein. Because K_i^{app} values are highly dependent on experimental conditions, we believe that our side-by-side comparison, derived from multiple independent experimental replicates, is likely to offer a more reliable comparison of the K_i^{app} values of this group of inhibitors.

Construction of a *M. smegmatis* strain with $MbtA_{tb}$-dependent susceptibility to salicyl-AMS.

The study of the antimicrobial properties of tuberculosis lead compounds using *Mtb* is challenging due to the need for biosafety level 3 procedures and the bacterium's slow growth rate. Thus, to simplify the analysis of the antimicrobial properties of $MbtA_{tb}$ inhibitors, we sought to use the nonpathogenic, fast-replicating *Msm* model system. *Msm* has the MBT siderophore system, and we have shown that the $MbtA_{tb}$ orthologue in *Msm* ($MbtA_{sm}$) (71% sequence identity) is essential for MBT biosynthesis.[8] However, *Msm* also has a second siderophore system that accounts for 90–95% of siderophore activity in the bacterium (*i.e.* the EXO system noted above).[71,72] We hypothesized that production of EXOs would render *Msm* resistant to salicyl-AMS (**1**), thus impeding the use of *Msm* for evaluation of MbtA inhibitors. To explore this view, we first investigated the susceptibility of *Msm* WT, *Msm* E (EXO^-, Figure S8A), and *Msm* M (MBT^-, Figure S8B) to salicyl-AMS (**1**) in Fe-limiting and Fe-rich growth media (Table 2). As expected, among these three strains, only *Msm* ΔE was susceptible, and the potent activity of salicyl-AMS (**1**) (MIC = 0.5–1 μg/mL) was exquisitely conditional to the Fe-limiting condition, a property consistent with its mechanism of action in inhibiting MBT siderophore biosynthesis. Under this condition, *Msm* ΔE relied on MBT production to acquire the Fe needed for growth, as indicated by the failure of *Msm* EM (EXO^-/MBT^-) to grow in the Fe-limiting medium (Table 2). This lack-of-growth phenotype, which is viewed as a reference for the effect of 100% pharmacological

inhibition of MbtA in *Msm* ΔE, was corrected in the complementation control strain with episomal expression of $mbtA_{sm}$ (Figure S8C), thus ruling out confounding mutations or polar effects in the double mutant. The lack of growth of the siderophore-deficient *Msm* ΔEM mutant in the Fe-limiting medium is in agreement with previous observations[73,74] and mimics the phenotype seen for *Mtb* MBT^- mutants.[12,15,17,74–76] In accordance with previous reports,[73,74] the growth defect of *Msm* ΔEM was corrected by addition of Fe to the culture medium (Figure S7C).

Notably, the lack of susceptibility seen with the EXO^+ strains under the Fe-limiting condition and with all strains under the Fe-rich condition indicated that salicyl-AMS (**1**) (at up to 1 mM, ≈1,000 × MIC; Table 2) does not have significant off-target effects in *Msm*. This finding contrasts with the observation that salicyl-AMS (**1**) (Table 2) and analogues **3a**, **3b**, **5a**, and **5b** (Table 3) have significant antimycobacterial activity against *Mtb* even in Fe-rich media (MIC values increased by only 4–64 fold relative to low-Fe medium).[23] The results obtained with *Mtb* have been attributed to off-target effects.[23] Alternatively, our review of the literature revealed that MBT-deficient mutants have been shown to display either a significant growth defect[17,74–77] or no defect[12,15] compared with WT when grown in iron-rich media. This difference is study-dependent, and suggests that MBT production might be needed for WT growth even in Fe-rich media, but only under some experimental conditions. This precludes determination of whether the *Mtb* growth inhibition resulting from MbtA inhibitors in the Fe-rich media is due to MBT inhibition, off-target effects, or a combination of both. Thus, the possibility of off-target effect confounders in *Mtb*-based SAR analyses of MbtA inhibitors cannot be ruled out, a disadvantage not found with the *Msm* model developed herein.

Collectively, the above results demonstrated that salicyl-AMS (**1**) has potent and selective antimicrobial activity against *Msm* ΔE. Encouraged by these results, we next explored the possibility of developing a *Msm* EXO^- strain that is dependent upon $MbtA_{tb}$, the primary intended target of salicyl-AMS (**1**). To this end, we transformed the *Msm* ΔEM double mutant with $pMbtA_{tb}$ to enable heterologous expression of $mbtA_{tb}$. We found that the transformant (*Msm* ΔEM-$pMbtA_{tb}$) regained MBT production (Figure S8B) and had the same pattern of susceptibility to salicyl-AMS (**1**) seen for *Msm* ΔE (Table 2 and Figure S8D). Moreover, salicyl-AMS (**1**) inhibited MBT production in *Msm* ΔEM-$pMbtA_{tb}$ (Figure S8B), a result paralleling that seen with *Mtb*.[6] Taken together, these results established that *Msm* ΔEM-$pMbtA_{tb}$ has high, $MbtA_{tb}$-dependent salicyl-AMS susceptibility, and thus the strain represents a convenient model system to assess and compare the antimycobacterial properties of the $MbtA_{tb}$ inhibitors.

Antimicrobial activity and post-antibiotic effect of salicyl-AMS and analogues.

To assess the antimycobacterial activity of our two novel $MbtA_{tb}$ inhibitors (**4b**, **6**) and to gain additional insight into the antibacterial properties of salicyl-AMS (**1**) and the six previously reported analogues (**2**, **3a**, **3b**, **4a**, **5a**, **5b**), we determined MIC values and investigated *in vitro* PAE using *Msm* EM-$pMbtA_{tb}$ (Table 3). Notably, despite the relevance of PAE information to the lead optimization and prioritization phases of antibiotic

development,[78–80] to our knowledge PAE studies have not been undertaken previously for salicyl-AMS (**1**) or any of its analogues.

Evaluation of antimicrobial activity in Fe-limiting media revealed MIC values in the 0.8–5.3 μg/mL range (≈6-fold relative spread), indicating that all of the $MtbA_{tb}$ inhibitors had potent activity against *Msm* ΔEM-pMbtA$_{tb}$. This narrow range parallels the modest, 11-fold relative spread observed for the K_i^{app} range (Table 1). The MIC value for salicyl-AMS (**1**) (0.8 μg/mL) was at the lowest end of the range, and none of the analogues displayed improved potency (Table 3), an outcome mirroring the results of the analysis of K_i^{app} values (Table 1). In this light, it is perhaps not surprising that Pearson correlation analysis revealed no statistically significant correlation between the antibacterial potency captured by the MIC dataset and the $MbtA_{tb}$ inhibitory potency informed by the K_i^{app} dataset (PCC < 0.5). The relatively small differences seen in *in vitro* potency are probably overpowered by the numerous cellular factors known to impact its translation into cell-based assay potency (*e.g.*, drug penetration/efflux/inactivation, non-specific off-target binding, target vulnerability/turnover, etc.),[79,81] and thus it is likely that any existing K_i^{app}-MIC correlation would have been confounded. On the other hand, lack of correlation between biochemical activity and whole-cell antimycobacterial activity is a well-known challenge in the tuberculosis drug development field, a phenomenon thought to arise from a mostly unpredictable combination of factors (*e.g.* penetration through the mycomembrane, intracellular metabolism, and extrusion by efflux pumps) differentially affecting each compound.[82–84]

Encouragingly, the results demonstrated potent antimicrobial activity for the novel analogues salicyl-AMSNMe (**4b**) and salicyl-6-MeO-AMSN (**6**). While *N*-methylsulfamide analogue **4b** had an MIC value indistinguishable from that of salicyl-AMS (**1**), 6-methoxy analogue **6** displayed a 6-fold decrease in potency compared to **1**. Among the previously reported analogues, we found no statistically significant difference between the MIC values of salicyl-AMS (**1**), salicyl-2-Ph-AMS (**3a**), salicyl-2-NHPh-AMS (**3b**), salicyl-AMSN (**4a**), and salicyl-6-*N*-Me-AMS (**5a**), whereas salicyl-2′-dAMS (**2**) and salicyl-6-*N*-*c*-Pr-AMS (**5b**) showed a significant 6-fold decrease in potency compared to **1** (Table 3). Notably, neither salicyl-AMS (**1**) nor the analogues reached MIC when tested at up to 1,000 and 64 μg/mL, respectively, in Fe-rich medium (Tables 2 and 3). This selectivity is consistent with their expected mechanism of action in inhibition of MBT siderophore biosynthesis, and revealed that the structural features of the analogues setting them apart from the lead compound **1** did not lead to unintended off-target effects of significance in *Msm.*

Notably, the MIC of 0.5–1 μg/ml found for salicyl-AMS (**1**) against *Msm* ΔEM-pMbtA$_{tb}$ is in reasonable agreement with the MIC of ≈0.1–0.5 μg/ml reported previously for *Mtb* in Fe-limiting medium, when using a bacterial inoculum level comparable to that herein.[23,24,33] The similarity between the MIC values of salicyl-AMS (**1**), salicyl-6-*N*-Me-AMS (**5a**), and salicyl-AMSN (**4a**) determined herein against *Msm* ΔEM-pMbtA$_{tb}$ is also in reasonable agreement with the MIC data reported with *Mtb*, considering the experimental variability of MIC assessments.[23,24] Notably, salicyl-2′-dAMS (**2**) displayed reduced activity in both bacterial species, but much more so in *Mtb*. This might be a consequence of the longer

incubation period of the MIC assay for *Mtb*, which could lead to some degradation of the less-stable 2′-deoxynucleoside structure.[28,85]

On the other hand, we found no statistically significant difference between the MIC value of salicyl-AMS (**1**) and those of adenine C2-substituted analogues **3a** and **3b** against *Msm* ΔEM-pMbtA$_{tb}$, in contrast to a previous report that these analogues are ten times more potent than **1** against *Mtb*. Moreover, we found salicyl-6-*N*-*c*-Pr-AMS (**5b**) to be six times less potent than salicyl-AMS (**1**) against *Msm* EM-pMbtA$_{tb}$, while this analogue was previously reported to be four times more potent than **1** against *Mtb*. Thus, there is only partial agreement between the MIC profiles of the inhibitor series emerging from testing against *Msm* and *Mtb*. The possibility that the increase in potency of analogues **3a**, **3b**, and **5b** relative to salicyl-AMS (**1**) seen in *Mtb* is due to an off-target effect cannot be ruled out. Alternatively, other species-specific factors and/or variations in the experimental conditions might have contributed to the differences.

Encouragingly, the assessment of the *in vitro* PAE, using washout experiments, revealed that all the inhibitors had a substantially delayed regrowth following inhibitor exposure (Table 3). A concentration-dependent PAE trend was found for the eight inhibitors tested at different concentrations, showing 0–14 h, 12–30 h, and 19–50 h ranges for the 5×, 50×, and 100× MIC exposures, respectively. For reference, drugs commonly used to treat tuberculosis have reported PAEs in the 2–68 h range[86] and drugs to treat infections with the fast-growing *Mycobacterium fortuitum* have PAEs in the 5–15 h range.[87] Within each inhibitor concentration evaluated, the majority of the PAE values of the analogues had no statistically significant difference from that of salicyl-AMS (**1**) (Table 3). A correlation between *in vitro* PAE and t_R datasets is occasionally seen for inhibitor series,[88] and thus we explored this possibility. Pearson pairwise correlation analysis revealed no significant correlation between the PAE and t_R datasets (PCC < 0.5). This is not surprising considering that the relatively modest t_R differences between the inhibitors are probably eclipsed by the various cellular factors influencing the extent of intracellular target engagement (*e.g.*, inhibitor penetration and efflux, target turnover, etc.),[79,81] and thus it is likely that any existing t_R–PAE correlation would have been confounded. In all, to our knowledge, these results provide the first demonstration of PAE for MbtA$_{tb}$ inhibitors. Moreover, they validate *Msm* ΔEM-pMbtA$_{tb}$ as a convenient model system for analyses of inhibitors of MbtA$_{tb}$.

CONCLUSIONS

Our analyses of salicyl-AMS and its analogues as MbtA$_{tb}$ inhibitors indicate that they all are potent, competitive TBIs, with a static, slow-onset inhibition mechanism, and a considerable t_R. The inhibitors are relatively similar to one another in terms of kinetic parameters. The fairly potent MbtA$_{tb}$ inhibition activity of the new analogue salicyl-6-MeO-AMSN (**6**) is unexpected based on previously published SAR and modeling analyses. Further SAR exploration of C6-substituents is therefore warranted. The second new analogue salicyl-AMSNMe (**4b**), which was designed to promote a favorable pharmacophoric *cisoid* conformation, has improved MbtA$_{tb}$ inhibitory potency compared with the unsubstituted counterpart. This observation highlights substitutions promoting a *cisoid* conformation as a topic deserving further investigation. Our evaluation of the antimicrobial properties of the

$MtbA_{tb}$ inhibitors were greatly facilitated by using a convenient *Msm*-based model system. This model is free of off-target effect confounders, whereas such confounders cannot be ruled out in SAR analyses of $MbtA_{tb}$ inhibitors using *Mtb*. All of these inhibitors have potent antimycobacterial activity and are similar to one another in terms of MIC values, a finding that parallels their relatively narrow range of K_i^{app} values. All of the inhibitors have also a substantial PAE, a clinically significant property shared with drugs commonly used against mycobacterial infections. This property, along with the long t_R of the inhibitors, may explain the efficacy of salicyl-AMS monotherapy in the murine model of tuberculosis using daily dosing (5.6 or 16.7 mg/kg), despite its relatively rapid clearance (lung half-life = 13 min after 50 mg/kg intraperitoneal administration).[33] The PAE and long t_R of salicyl-AMS suggest retention of the compound at the target site during the efficacy studies, which would not be detected in the pharmacokinetic studies where there are no bacteria to maintain the compound in the lung. In all, the insights gained in the present study support the advancement of the new analogues to testing in *Mtb* strains and set the stage for further preclinical evaluation of pharmacological and toxicological properties to identify the most promising candidates for evaluation of *in vivo* efficacy in mouse models of tuberculosis.

Supplementary Material

Refer to Web version on PubMed Central for supplementary material.

ACKNOWLEDGMENT

We thank Omar Omar (L.E.N.Q. laboratory) for assistance with mutant constructions and Lukman Solola (L.E.N.Q. laboratory) for help with CAS-Q assays. We thank Yasutomi Asano (Takeda), Makoto Fushimi (Takeda), Naoyoshi Noguchi (Takeda), and Michael A. Foley (Tri-Institutional Therapeutics Discovery Institute) for assistance with the synthesis of salicyl-AMS.

Funding Sources

This work was supported in part by the National Institutes of Health (R01 AI118224 to D.S.T. and L.E.N.Q., F31 AI129244 to L.C.S., CCSG P30 CA008748 to C. B. Thompson), the Tri-Institutional Therapeutics Discovery Institute, and endowment support from Carol and Larry Zicklin to L.E.N.Q.

REFERENCES

(1). Global tuberculosis report 2017 Geneva: World Health Organization (2017). Licence: CC BY-NCSA 3.0 IGO.

(2). Barry CE 3rd, and Mdluli K (1996) Drug sensitivity and environmental adaptation of mycobacterial cell wall components. Trends Microbiol 4, 275–281. [PubMed: 8829336]

(3). Nahid P, Dorman SE, Alipanah N, Barry PM, Brozek JL, Cattamanchi A, Chaisson LH, Chaisson RE, Daley CL, Grzemska M, Higashi JM, Ho CS, Hopewell PC, Keshavjee SA, Lienhardt C, et al. (2016) Official american thoracic society/centers for disease control and prevention/infectious diseases society of america clinical practice guidelines: Treatment of drug-susceptible tuberculosis. Clin. Infect. Dis 63, e147–e195. [PubMed: 27516382]

(4). Alipanah N, Jarlsberg L, Miller C, Linh NN, Falzon D, Jaramillo E, and Nahid P (2018) Adherence interventions and outcomes of tuberculosis treatment: A systematic review and meta-analysis of trials and observational studies. PLoS Med 15, e1002595. [PubMed: 29969463]

(5). Awofeso N Anti-tuberculosis medication side-effects constitute major factor for poor adherence to tuberculosis treatment, Bull. World Health Organ 2008 3;86(3):B-D.

(6). Ferreras JA, Ryu JS, Di Lello F, Tan DS, and Quadri LE (2005) Small-molecule inhibition of siderophore biosynthesis in *Mycobacterium tuberculosis* and *Yersinia pestis*. Nat. Chem. Biol 1, 29–32. [PubMed: 16407990]

(7). Quadri LE, Sello J, Keating TA, Weinreb PH, and Walsh CT (1998) Identification of a *Mycobacterium tuberculosis* gene cluster encoding the biosynthetic enzymes for assembly of the virulence-conferring siderophore mycobactin. Chem. Biol 5, 631–645. [PubMed: 9831524]

(8). Chavadi SS, Stirrett KL, Edupuganti UR, Sadhanandan G, Vergnolle O, Schumacher E, Martin C, Qiu WG, Soll CE, and Quadri LEN (2011) Mutational and phylogenetic analyses of the mycobacterial *mbt* gene cluster. J. Bacteriol 193, 5905–5913. [PubMed: 21873494]

(9). Quadri LEN, and Ratledge C (2005) Iron metabolism in the tubercle bacillus and other mycobacteria, In Tuberculosis and the Tubercle Bacillus (Cole ST, Eisenach KD, McMurray DN, et al., Eds.), pp 341–357, ASM Press, Washington, DC.

(10). Ratledge C (2004) Iron, mycobacteria and tuberculosis. Tuberculosis (Edinb) 84, 110–130. [PubMed: 14670352]

(11). De Voss JJ, Rutter K, Schroeder BG, and Barry CE 3rd. (1999) Iron acquisition and metabolism by mycobacteria. J. Bacteriol 181, 4443–4451. [PubMed: 10419938]

(12). De Voss JJ, Rutter K, Schroeder BG, Su H, Zhu Y, and Barry CE 3rd. (2000) The salicylate-derived mycobactin siderophores of *Mycobacterium tuberculosis* are essential for growth in macrophages. Proc. Natl. Acad. Sci. U.S.A 97, 1252–1257. [PubMed: 10655517]

(13). Rodriguez GM, and Smith I (2006) Identification of an ABC transporter required for iron acquisition and virulence in *Mycobacterium tuberculosis*. J. Bacteriol 188, 424–430. [PubMed: 16385031]

(14). Reddy PV, Puri RV, Chauhan P, Kar R, Rohilla A, Khera A, and Tyagi AK (2013) Disruption of mycobactin biosynthesis leads to attenuation of *Mycobacterium tuberculosis* for growth and virulence. J. Infect. Dis 208, 1255–1265. [PubMed: 23788726]

(15). Madigan CA, Martinot AJ, Wei JR, Madduri A, Cheng TY, Young DC, Layre E, Murry JP, Rubin EJ, and Moody DB (2015) Lipidomic analysis links mycobactin synthase K to iron uptake and virulence in *M. tuberculosis*. PLoS Pathog 11, e1004792. [PubMed: 25815898]

(16). Wells RM, Jones CM, Xi Z, Speer A, Danilchanka O, Doornbos KS, Sun P, Wu F, Tian C, and Niederweis M (2013) Discovery of a siderophore export system essential for virulence of *Mycobacterium tuberculosis*. PLoS Pathog 9, e1003120. [PubMed: 23431276]

(17). Tufariello JM, Chapman JR, Kerantzas CA, Wong KW, Vilcheze C, Jones CM, Cole LE, Tinaztepe E, Thompson V, Fenyo D, Niederweis M, Ueberheide B, Philips JA, and Jacobs WR Jr. (2016) Separable roles for *Mycobacterium tuberculosis* ESX-3 effectors in iron acquisition and virulence. Proc. Natl. Acad. Sci. U. S. A 113, E348–357. [PubMed: 26729876]

(18). Quadri LE (2007) Strategic paradigm shifts in the antimicrobial drug discovery process of the 21st century. Infect. Disord. Drug Targets 7, 230–237. [PubMed: 17897059]

(19). Meneghetti F, Villa S, Gelain A, Barlocco D, Chiarelli LR, Pasca MR, and Costantino L (2016) Iron acquisition pathways as targets for antitubercular drugs. Curr. Med. Chem 23, 4009–4026. [PubMed: 27281295]

(20). Monfeli RR, and Beeson C (2007) Targeting iron acquisition by *Mycobacterium tuberculosis*. Infect. Disord. Drug Targets 7, 213–220. [PubMed: 17897057]

(21). Gehring AM, Mori I, Perry RD, and Walsh CT (1998) The nonribosomal peptide synthetase HMWP2 forms a thiazoline ring during biogenesis of yersiniabactin, an iron-chelating virulence factor of *Yersinia pestis*. Biochemistry 37, 11637–11650. [PubMed: 9709002]

(22). Quadri LE, Keating TA, Patel HM, and Walsh CT (1999) Assembly of the *Pseudomonas aeruginosa* nonribosomal peptide siderophore pyochelin: *in vitro* reconstitution of aryl-4,2-bis-thiazoline synthetase activity from PchD, PchE, and PchF. Biochemistry 38, 14941–14954. [PubMed: 10555976]

(23). Neres J, Labello NP, Somu RV, Boshoff HI, Wilson DJ, Vannada J, Chen L, Barry CE 3rd, Bennett EM, and Aldrich CC (2008) Inhibition of siderophore biosynthesis in *Mycobacterium tuberculosis* with nucleoside bisubstrate analogues: structure-activity relationships of the nucleobase domain of 5'-*O*-[*N*-(salicyl)sulfamoyl]adenosine. J. Med. Chem 51, 5349–5370. [PubMed: 18690677]

(24). Somu RV, Boshoff H, Qiao C, Bennett EM, Barry CE 3rd, and Aldrich CC (2006) Rationally designed nucleoside antibiotics that inhibit siderophore biosynthesis of *Mycobacterium tuberculosis*. J. Med. Chem 49, 31–34. [PubMed: 16392788]

(25). Somu RV, Wilson DJ, Bennett EM, Boshoff HI, Celia L, Beck BJ, Barry CE 3rd, and Aldrich CC (2006) Antitubercular nucleosides that inhibit siderophore biosynthesis: SAR of the glycosyl domain. J. Med. Chem 49, 7623–7635. [PubMed: 17181146]

(26). Vannada J, Bennett EM, Wilson DJ, Boshoff HI, Barry CE 3rd, and Aldrich CC (2006) Design, synthesis, and biological evaluation of β-ketosulfonamide adenylation inhibitors as potential antitubercular agents. Org. Lett 8, 4707–4710. [PubMed: 17020283]

(27). Nelson KM, Viswanathan K, Dawadi S, Duckworth BP, Boshoff HI, Barry CE 3rd, and Aldrich CC (2015) Synthesis and pharmacokinetic evaluation of siderophore biosynthesis inhibitors for *Mycobacterium tuberculosis*. J. Med. Chem 58, 5459–5475. [PubMed: 26110337]

(28). Duckworth BP, Nelson KM, and Aldrich CC (2012) Adenylating enzymes in *Mycobacterium tuberculosis* as drug targets. Curr. Top. Med. Chem 12, 766–796. [PubMed: 22283817]

(29). Dawadi S, Boshoff HIM, Park SW, Schnappinger D, and Aldrich CC (2018) Conformationally constrained cinnolinone nucleoside analogues as siderophore biosynthesis inhibitors for tuberculosis. ACS Med. Chem. Lett 9, 386–391. [PubMed: 29670706]

(30). Engelhart CA, and Aldrich CC (2013) Synthesis of chromone, quinolone, and benzoxazinone sulfonamide nucleosides as conformationally constrained inhibitors of adenylating enzymes required for siderophore biosynthesis. J. Org. Chem 78, 7470–7481. [PubMed: 23805993]

(31). Dawadi S, Kawamura S, Rubenstein A, Remmel R, and Aldrich CC (2016) Synthesis and pharmacological evaluation of nucleoside prodrugs designed to target siderophore biosynthesis in *Mycobacterium tuberculosis*. Bioorg. Med. Chem. Lett 24, 1314–1321.

(32). Krajczyk A, Zeidler J, Januszczyk P, Dawadi S, Boshoff HI, Barry CE 3rd, Ostrowski T, and Aldrich CC (2016) 2-Aryl-8-aza-3-deazaadenosine analogues of 5'-O-[*N*-(salicyl)sulfamoyl]adenosine: Nucleoside antibiotics that block siderophore biosynthesis in *Mycobacterium tuberculosis*. Bioorg. Med. Chem. Lett 24, 3133–3143.

(33). Lun S, Guo H, Adamson J, Cisar JS, Davis TD, Chavadi SS, Warren JD, Quadri LE, Tan DS, and Bishai WR (2013) Pharmacokinetic and *in vivo* efficacy studies of the mycobactin biosynthesis inhibitor salicyl-AMS in mice. Antimicrob. Agents Chemother 57, 5138–5140. [PubMed: 23856770]

(34). Sambrook J, Russell DW (2001) Molecular cloning: A laboratory manual, 3rd ed., Cold Spring Harbor Press, Cold Spring Harbor, NY.

(35). Wilson DJ, and Aldrich CC (2010) A continuous kinetic assay for adenylation enzyme activity and inhibition. Anal. Biochem 404, 56–63. [PubMed: 20450872]

(36). Davis TD, Mohandas P, Chiriac MI, Bythrow GV, Quadri LE, and Tan DS (2016) Design, synthesis, and biological evaluation of -hydroxyacyl-AMS inhibitors of amino acid adenylation enzymes. Bioorg. Med. Chem. Lett 26, 5340–5345. [PubMed: 27692545]

(37). Copeland RA (2013) Tight binding inhibition, In Evaluation of enzyme inhibitors in drug discovery, pp 245–285, John Wiley & Sons, Inc.

(38). Brooks HB, Geeganage S, Kahl SD, Montrose C, Sittampalam S, Smith MC, and Weidner JR (2004) Basics of enzymatic assays for HTS, In Assay guidance manual (Sittampalam GS, Coussens NP, Brimacombe K, et al., Eds.), Bethesda (MD).

(39). Copeland RA (2002) Tight binding inhibitors, In Enzymes, pp 305–317, John Wiley & Sons, Inc.

(40). Murphy DJ (2004) Determination of accurate KI values for tight-binding enzyme inhibitors: An in silico study of experimental error and assay design. Anal. Biochem 327, 61–67. [PubMed: 15033511]

(41). Sikora AL, Wilson DJ, Aldrich CC, and Blanchard JS (2010) Kinetic and inhibition studies of dihydroxybenzoate-AMP ligase (EntE) from Escherichia coli. Biochemistry 49, 3648–3657. [PubMed: 20359185]

(42). McClerren AL, Endsley S, Bowman JL, Andersen NH, Guan Z, Rudolph J, and Raetz CR (2005) A slow, tight-binding inhibitor of the zinc-dependent deacetylase LpxC of lipid A biosynthesis with antibiotic activity comparable to ciprofloxacin. Biochemistry 44, 16574–16583. [PubMed: 16342948]

(43). Morrison JF, and Walsh CT (1988) The behavior and significance of slow-binding enzyme inhibitors. Adv. Enzymol. Relat. Areas Mol. Biol 61, 201–301. [PubMed: 3281418]

(44). Copeland RA (2013) Slow binding inhibitors, In Evaluation of enzyme inhibitors in drug discovery, pp 203–244, John Wiley & Sons, Inc.

(45). Chang A, Schiebel J, Yu W, Bommineni GR, Pan P, Baxter MV, Khanna A, Sotriffer CA, Kisker C, and Tonge PJ (2013) Rational optimization of drug-target residence time: Insights from inhibitor binding to the *Staphylococcus aureus* FabI enzyme-product complex. Biochemistry 52, 4217–4228. [PubMed: 23697754]

(46). Larionova NI, Gladysheva IP, and Gladyshev DP (1997) Human leukocyte elastase inhibition by Bowman-Birk soybean inhibitor. Discrimination of the inhibition mechanisms. FEBS Lett 404, 245–248. [PubMed: 9119072]

(47). Snapper SB, Melton RE, Mustafa S, Kieser T, and Jacobs WR Jr. (1990) Isolation and characterization of efficient plasmid transformation mutants of *Mycobacterium smegmatis*. Mol. Microbiol 4, 1911–1919. [PubMed: 2082148]

(48). Ferreras JA, Gupta A, Amin ND, Basu A, Sinha BN, Worgall S, Jayaprakash V, and Quadri LE (2011) Chemical scaffolds with structural similarities to siderophores of nonribosomal peptide-polyketide origin as novel antimicrobials against *Mycobacterium tuberculosis* and *Yersinia pestis*. Bioorg. Med. Chem. Lett 21, 6533–6537. [PubMed: 21940166]

(49). Parish T, and Stoker NG (2000) Use of a flexible cassette method to generate a double unmarked *Mycobacterium tuberculosis tlyA plcABC* mutant by gene replacement. Microbiology 146, 1969–1975. [PubMed: 10931901]

(50). Mohan A, Padiadpu J, Baloni P, and Chandra N (2015) Complete genome sequences of a Mycobacterium smegmatis laboratory strain (MC^2 155) and isoniazid-resistant (4XR1/R2) mutant strains. Genome Announc 3.

(51). Fiss EH, Yu S, and Jacobs WR Jr. (1994) Identification of genes involved in the sequestration of iron in mycobacteria: The ferric exochelin biosynthetic and uptake pathways. Mol. Microbiol 14, 557–569. [PubMed: 7885234]

(52). Yu S, Fiss E, and Jacobs WR Jr. (1998) Analysis of the exochelin locus in *Mycobacterium smegmatis*: Biosynthesis genes have homology with genes of the peptide synthetase family. J. Bacteriol 180, 4676–4685. [PubMed: 9721311]

(53). Zhu W, Arceneaux JE, Beggs ML, Byers BR, Eisenach KD, and Lundrigan MD (1998) Exochelin genes in *Mycobacterium smegmatis*: Identification of an ABC transporter and two non-ribosomal peptide synthetase genes. Mol. Microbiol 29, 629–639. [PubMed: 9720878]

(54). Ma J, Campbell A, and Karlin S (2002) Correlations between Shine-Dalgarno sequences and gene features such as predicted expression levels and operon structures. J. Bacteriol 184, 5733–5745. [PubMed: 12270832]

(55). Ferreras JA, Stirrett KL, Lu X, Ryu JS, Soll CE, Tan DS, and Quadri LE (2008) Mycobacterial phenolic glycolipid virulence factor biosynthesis: Mechanism and small-molecule inhibition of polyketide chain initiation. Chem. Biol 15, 51–61. [PubMed: 18158259]

(56). Stirrett KL, Ferreras JA, Jayaprakash V, Sinha BN, Ren T, and Quadri LE (2008) Small molecules with structural similarities to siderophores as novel antimicrobials against *Mycobacterium tuberculosis* and *Yersinia pestis*. Bioorg. Med. Chem. Lett 18, 2662–2668. [PubMed: 18394884]

(57). Chan CY, Au-Yeang C, Yew WW, Leung CC, and Cheng AF (2004) *In vitro* postantibiotic effects of rifapentine, isoniazid, and moxifloxacin against *Mycobacterium tuberculosis*. Antimicrob. Agents Chemother 48, 340–343. [PubMed: 14693563]

(58). Stubbings WJ, Bostock JM, Ingham E, and Chopra I (2004) Assessment of a microplate method for determining the post-antibiotic effect in *Staphylococcus aureus* and *Escherichia coli*. J. Antimicrob. Chemother 54, 139–143. [PubMed: 15150167]

(59). Khan F, He M, and Taussig MJ (2006) Double-hexahistidine tag with high-affinity binding for protein immobilization, purification, and detection on Ni-nitrilotriacetic acid surfaces. Anal. Chem 78, 3072–3079. [PubMed: 16642995]

(60). Lee J, and Kim SH (2009) High-throughput T7 LIC vector for introducing C-terminal poly-histidine tags with variable lengths without extra sequences. Protein Expr. Purif 63, 58–61. [PubMed: 18824233]

(61). Quadri LE (2000) Assembly of aryl-capped siderophores by modular peptide synthetases and polyketide synthases. Mol. Microbiol 37, 1–12. [PubMed: 10931301]

(62). Gulick AM (2009) Conformational dynamics in the acyl-CoA synthetases, adenylation domains of non-ribosomal peptide synthetases, and firefly luciferase. ACS Chem. Biol 4, 811–827. [PubMed: 19610673]

(63). Fromm HJ (1995) Reversible enzyme inhibitors as mechanistic probes. Methods Enzymol 249, 123–143. [PubMed: 7791609]

(64). May JJ, Kessler N, Marahiel MA, and Stubbs MT (2002) Crystal structure of DhbE, an archetype for aryl acid activating domains of modular nonribosomal peptide synthetases. Proc. Natl. Acad. Sci. U. S. A 99, 12120–12125. [PubMed: 12221282]

(65). Cisar JS, Ferreras JA, Soni RK, Quadri LE, and Tan DS (2007) Exploiting ligand conformation in selective inhibition of non-ribosomal peptide synthetase amino acid adenylation with designed macrocyclic small molecules. J. Am. Chem. Soc 129, 7752–7753. [PubMed: 17542590]

(66). Tawari NR, and Degani MS (2011) Predictive models for nucleoside bisubstrate analogs as inhibitors of siderophore biosynthesis in *Mycobacterium tuberculosis*: pharmacophore mapping and chemometric QSAR study. Mol. Divers 15, 435–444. [PubMed: 20306296]

(67). Labello NP, Bennett EM, Ferguson DM, and Aldrich CC (2008) Quantitative three dimensional structure linear interaction energy model of 5'-O-[*N*-(salicyl)sulfamoyl]adenosine and the aryl acid adenylating enzyme MbtA. J. Med. Chem 51, 7154–7160. [PubMed: 18959400]

(68). Maganti L, Open Source Drug Discovery, C., and Ghoshal N. (2014) Probing the structure of *Mycobacterium tuberculosis* MbtA: model validation using molecular dynamics simulations and docking studies. J. Biomol. Struct. Dyn 32, 273–288. [PubMed: 23527569]

(69). Copeland RA (2013) Drug–target residence time, In Evaluation of enzyme inhibitors in drug discovery, pp 287–344, John Wiley & Sons, Inc.

(70). Nunez S, Venhorst J, and Kruse CG (2012) Target-drug interactions: First principles and their application to drug discovery. Drug Discov. Today 17, 10–22. [PubMed: 21777691]

(71). Ratledge C, and Ewing M (1996) The occurrence of carboxymycobactin, the siderophore of pathogenic mycobacteria, as a second extracellular siderophore in *Mycobacterium smegmatis*. Microbiology 142, 2207–2212. [PubMed: 8800816]

(72). Sharman GJ, Williams DH, Ewing DF, and Ratledge C (1995) Isolation, purification and structure of exochelin MS, the extracellular siderophore from *Mycobacterium smegmatis*. Biochem. J 305, 187–196. [PubMed: 7826328]

(73). Siegrist MS, Unnikrishnan M, McConnell MJ, Borowsky M, Cheng TY, Siddiqi N, Fortune SM, Moody DB, and Rubin EJ (2009) Mycobacterial Esx-3 is required for mycobactin-mediated iron acquisition. Proc. Natl. Acad. Sci. U. S. A 106, 18792–18797. [PubMed: 19846780]

(74). Jones CM, Wells RM, Madduri AV, Renfrow MB, Ratledge C, Moody DB, and Niederweis M (2014) Self-poisoning of *Mycobacterium tuberculosis* by interrupting siderophore recycling. Proc. Natl. Acad. Sci. U. S. A 111, 1945–1950. [PubMed: 24497493]

(75). Jones CM, and Niederweis M (2011) *Mycobacterium tuberculosis* can utilize heme as an iron source. J. Bacteriol 193, 1767–1770. [PubMed: 21296960]

(76). Madigan CA, Cheng TY, Layre E, Young DC, McConnell MJ, Debono CA, Murry JP, Wei JR, Barry CE 3rd, Rodriguez GM, Matsunaga I, Rubin EJ, and Moody DB (2012) Lipidomic discovery of deoxysiderophores reveals a revised mycobactin biosynthesis pathway in *Mycobacterium tuberculosis*. Proc. Natl. Acad. Sci. U. S. A 109, 1257–1262. [PubMed: 22232695]

(77). Sassetti CM, Boyd DH, and Rubin EJ (2003) Genes required for mycobacterial growth defined by high density mutagenesis. Mol. Microbiol 48, 77–84. [PubMed: 12657046]

(78). Craig WA (2007) Pharmacodynamics of antimicrobials: General concepts and applications, In Antimicrobial pharmacodynamics in theory and clinical practice (Nightingale CH, Ambrose PG, Drusano GL, et al., Eds.) 2nd ed., pp 1–22, Informa Healthcare USA, Inc., New York, NY.

(79). Tonge PJ (2018) Drug-target kinetics in drug discovery. ACS Chem. Neurosci 9, 29–39. [PubMed: 28640596]

(80). MacKenzie FM, and Gould IM (1993) The post-antibiotic effect. J. Antimicrob. Chemother 32, 519–537. [PubMed: 8288494]

(81). Davis TD, Gerry CJ, and Tan DS (2014) General platform for systematic quantitative evaluation of small-molecule permeability in bacteria. ACS Chem. Biol 9, 2535–2544. [PubMed: 25198656]

(82). Singh V, and Mizrahi V (2017) Identification and validation of novel drug targets in *Mycobacterium tuberculosis*. Drug Discov. Today 22, 503–509. [PubMed: 27649943]

(83). Sharma U (2011) Current possibilities and unresolved issues of drug target validation in *Mycobacterium tuberculosis*. Expert Opin. Drug Discov 6, 1171–1186. [PubMed: 22646985]

(84). Machado D, Girardini M, Viveiros M, and Pieroni M (2018) Challenging the drug-likeness dogma for new drug discovery in tuberculosis. Front. Microbiol 9, 1367. [PubMed: 30018597]

(85). Lindahl T (1993) Instability and decay of the primary structure of DNA. Nature 362, 709–715. [PubMed: 8469282]

(86). Chan CY, Au-Yeang C, Yew WW, Hui M, and Cheng AF (2001) Postantibiotic effects of antituberculosis agents alone and in combination. Antimicrob. Agents Chemother 45, 3631–3634. [PubMed: 11709357]

(87). Tsui SY, Yew WW, Li MS, Chan CY, and Cheng AF (1993) Postantibiotic effects of amikacin and ofloxacin on *Mycobacterium fortuitum*. Antimicrob. Agents Chemother 37, 1001–1003. [PubMed: 8517688]

(88). Walkup GK, You Z, Ross PL, Allen EK, Daryaee F, Hale MR, O'Donnell J, Ehmann DE, Schuck VJ, Buurman ET, Choy AL, Hajec L, Murphy-Benenato K, Marone V, Patey SA, et al. (2015) Translating slow-binding inhibition kinetics into cellular and *in vivo* effects. Nat. Chem. Biol 11, 416–423. [PubMed: 25894085]

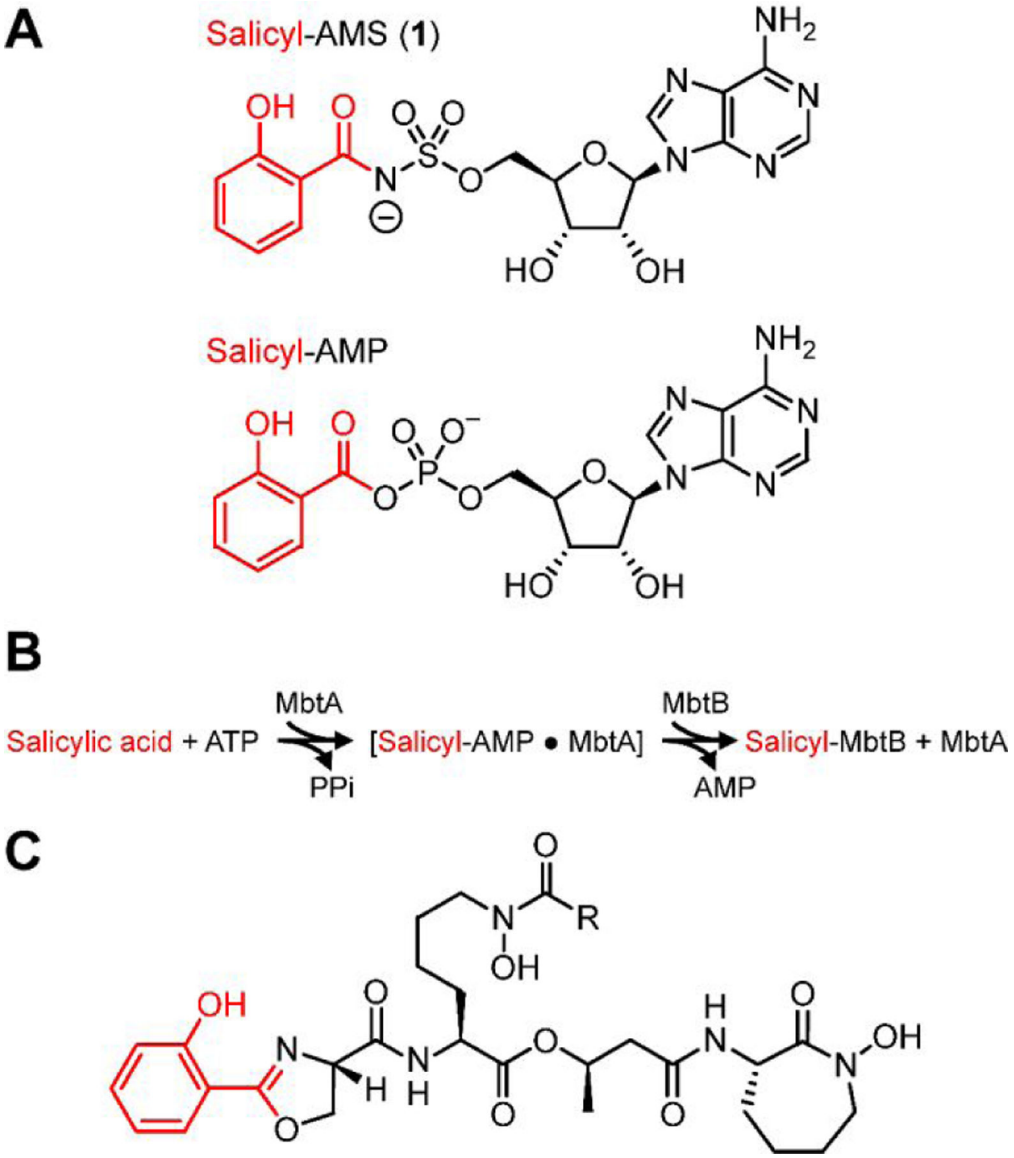

Figure 1.

(A) Nucleoside antibiotic salicyl-AMS and salicyl-AMP intermediate synthesized by the salicylate adenylation enzyme activity of $MbtA_{tb}$. **(B)** Reactions catalyzed by $MbtA_{tb}$ during mycobactin (MBT) biosynthesis. $MbtA_{tb}$ catalyzes formation of the first covalent acyl-enzyme intermediate during MBT acyl-chain assembly through a mechanism involving two-half reactions. The first half reaction is the ATP-dependent adenylation of salicylic acid to generate a salicyl-AMP intermediate that remains non-covalently bound to the active site. The second half-reaction is the transfer of the salicyl moiety of the adenylate onto the phosphopantetheinyl group of the carrier protein domain of the peptide synthetase MbtB. **(C)** Representative mycobactin siderophores of *M. tuberculosis*. R represents variable fatty acyl groups (mycobactin variants) or acyl substituents terminating in a carboxylate or a methyl ester (carboxymycobactin variants). All of these variants are herein collectively referred to as MBTs.

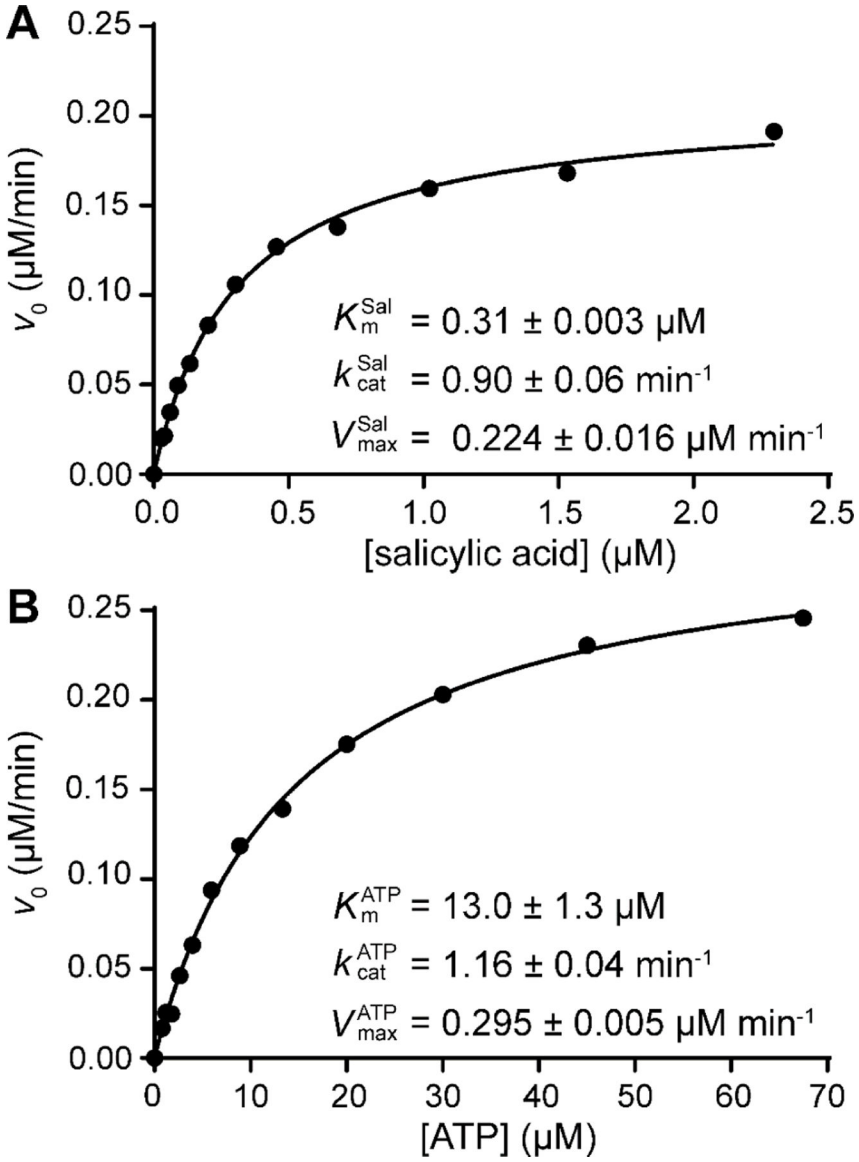

Figure 2.

Michaelis−Menten kinetic parameters for $H_{10}MbtA^{opt}$. The v_0 vs. [S] datasets were generated using salicylic acid **(A)** or ATP **(B)** as the variable substrate. Each plot shown is representative of two independent experiments. The datasets (●) were fitted to Eq. 1 to generate the solid line (R^2 values ≥ 0.993). The kinetic parameters indicated are mean values ± SEM of $n = 2$ independent experiments.

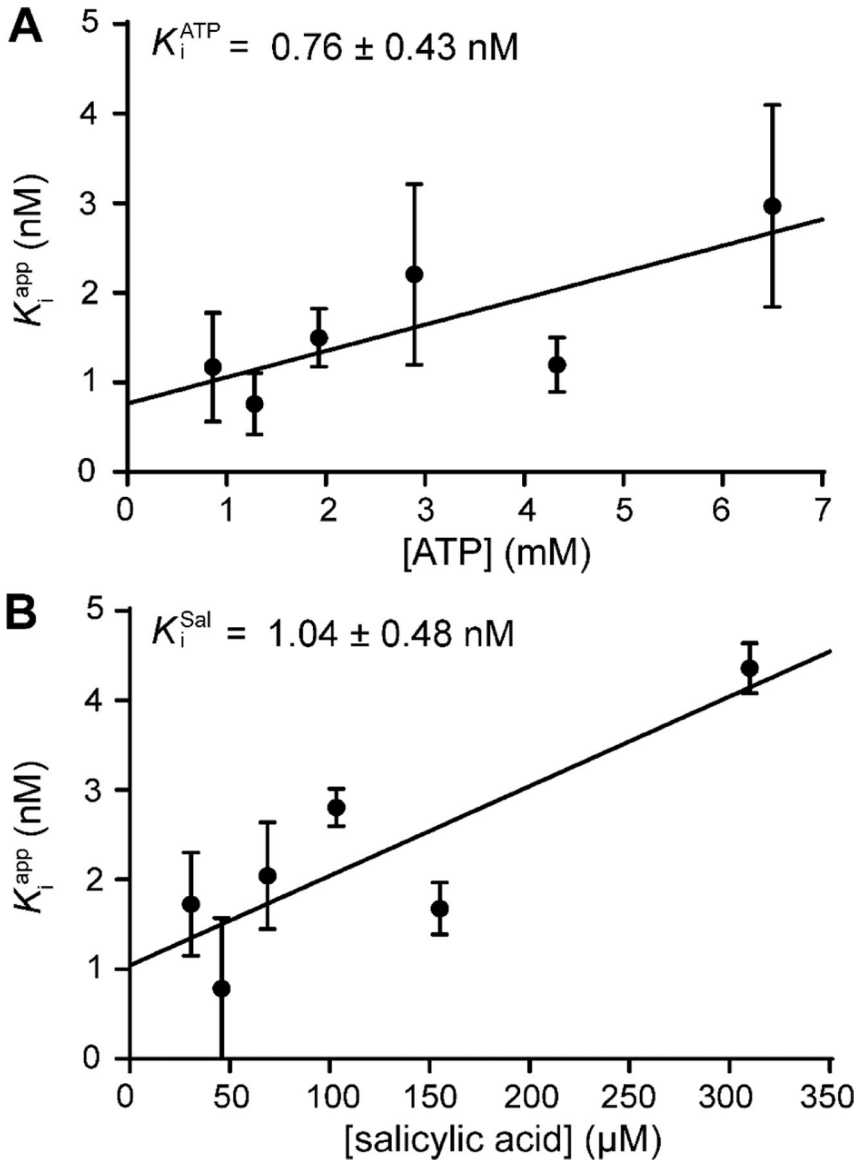

Figure 3.

K_i value of salicyl-AMS for $H_{10}MbtA^{opt}$ inhibition. Two K_i values were independently calculated using two approaches having opposite relationship of constant versus variable substrate. The K_i^{ATP} value **(A)** and K_i^{sal} value **(B)** were calculated from datasets of K_i^{app} values vs. ATP and salicylic acid concentration, respectively, as the *y*-intercept of the linear regression of the data (●) fitted to Eq. 3 (solid line; R^2 values ≥ 0.6). The K_i values indicated were calculated from the average of K_i^{app} vs. variable substrate datasets generated from three independent experiments. Error bars on K_i^{app} data points represent SEM of $n = 3$.

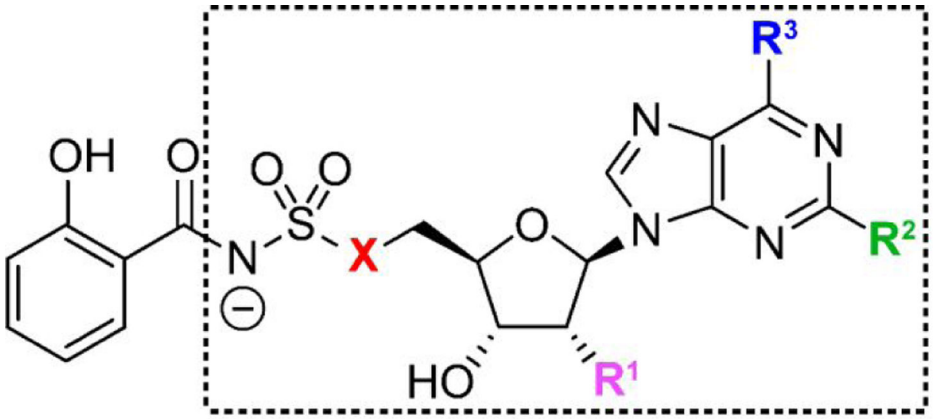

Cmpd.	X	R^1	R^2	R^3
1	O	OH	H	NH_2
2	O	H	H	NH_2
3a	O	OH	Ph	NH_2
3b	O	OH	NH-Ph	NH_2
4a	N	OH	H	NH_2
4b	N-Me	OH	H	NH_2
5a	O	OH	H	NH-Me
5b	O	OH	H	NH-*c*-Pr
6	N	OH	H	O-Me

Figure 4.

Structural differences between salicyl-AMS (**1**) and its various analogues with modifications in the AMS moiety (dotted line box) evaluated herein. Me, methyl; Ph, phenyl; *c*-Pr, cyclopropyl.

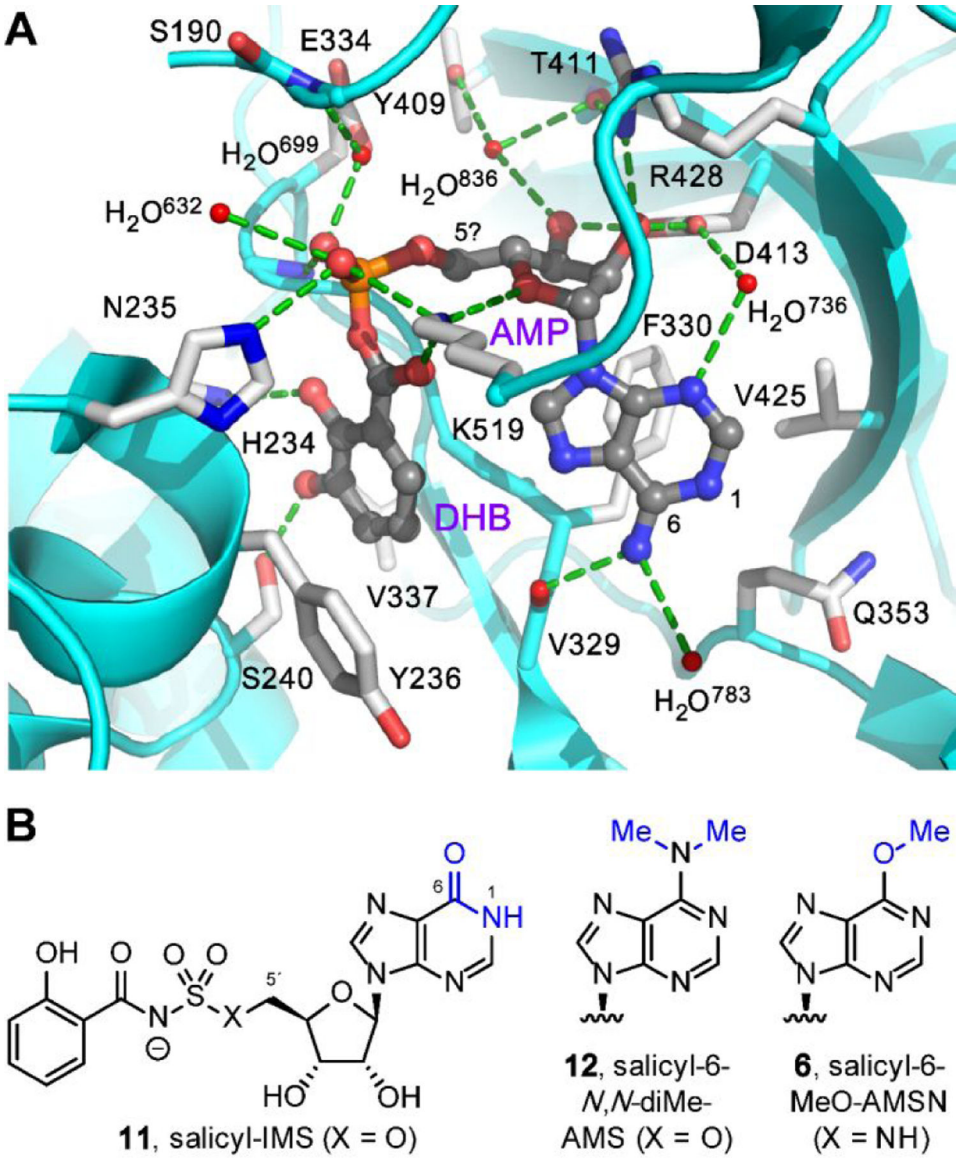

Figure 5.

Design rationales for new salicyl-AMS analogues. **(A)** Cocrystal structure of 2,3-dihydroxybenzoyl-AMP (DHB-AMP, gray) bound in the active site of the DHBA adenylation enzyme *Bacillus subtilis* DhbE (cyan and white, PDB: 1MDB),[64] illustrating pharmacophoric *cisoid* binding conformation.[65] Salicyl-AMSNMe (**4b**) is designed to promote this *cisoid* binding conformation. **(B)** Structures of previously reported inosine analogue salicyl-IMS (**11**) and dimethylated analogue salicyl-6-*N*,*N*-diMe-AMS (**12**), both of which are weak $MbtA_{tb}$ inhibitors,[23] presumably due to loss of hydrogen-bonding interaction with the main-chain carbonyl oxygen of $MbtA_{tb}$ V352 (DhbE V329). Salicyl-6-MeO-AMS (**6**) is designed to remove this hydrogen-bonding interaction without introducing a proton at N1 via tautomerization (*cf.* **11**) and without introducing a potential steric clash with V352 (*cf.* **12**).

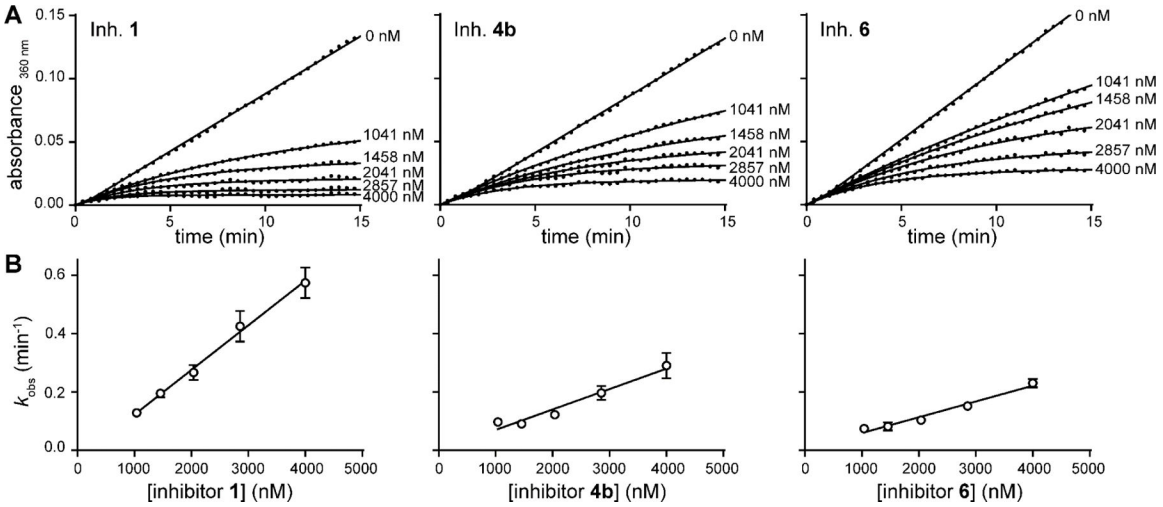

Figure 6.

Representative data for the kinetics of time-dependent inhibition of $H_{10}MbtA^{opt}$. **(A)** Progress curves for $MbtA_{tb}$ inhibition by different concentrations of **1**, **4b**, and **6**. The inhibitor number is indicated on the upper left corner of the plot. Each plot is representative of at least five independent experiments. The solid lines represent curve fitting to the dataset (●) using Eq. 4 to extract k_{obs} values. The R^2 values for ≈270 progress curves generated were in the 0.789–0.999 range, with an average of 0.985 and a median of 0.995, demonstrating excellent fit for the large majority of the curves. **(B)** Datasets showing the dependence of the extracted k_{obs} on the concentration of **1**, **4b**, and **6**. The datasets (●) were fitted to Eq. 7 to generate the solid lines (R^2 values ≥ 0.955). k_{obs} datapoints represent mean values ± SEM of $n \geq 5$ independent experiments.

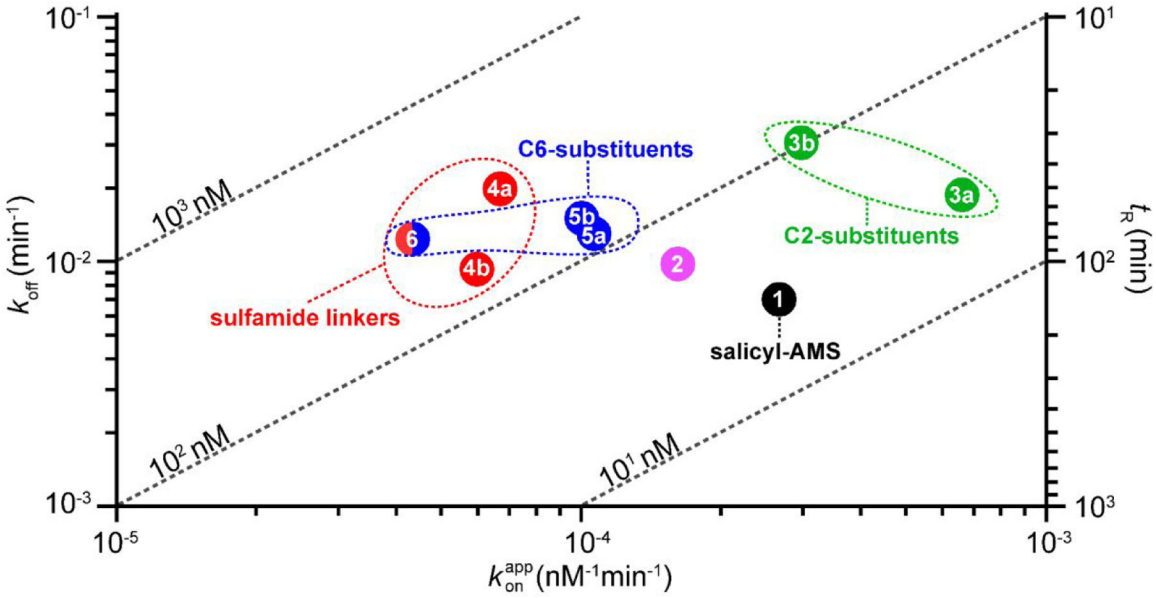

Figure 7.

Two-dimensional kinetic map for salicyl-AMS and its analogues. The map represents the data summarized in Table 1 and facilitates visualization of relationships between inhibitors and the kinetic parameters k_{off}, k_{on}^{app}, t_R, and K_i^{app} (diagonal dashed lines) noted in the text. The clustering of analogues with sulfamide-based linkers (**4a**, **4b**, **6**; red oval), modifications at C2 (**3a**, **3b**; green oval), and modifications at C6 (**5a**, **5b**, **6**; blue oval) is indicated.

Table 1.

Kinetic parameters for inhibitors of $MbtA_{tb}$

Cmpd.	IC_{50} (nM)[a]	K_i^{app} (nM)	k_{on}^{app} ($nM^{-1}min^{-1}$)	k_{off} (min^{-1})	t_R (min)
1	117.2 ± 0.3	26.6 ± 2.5	0.00027 ± 0.00003	0.007 ± 0.001	157 ± 22
2	153.6 ± 2.5*[b]	62.1 ± 5.0***	0.00016 ± 0.00002*	0.010 ± 0.001	109 ± 13
3a	150.9 ± 7.8	26.6 ± 6.4	0.00066 ± 0.00012*	0.019 ± 0.005*	76 ± 24*
3b	226.0 ± 3.0***	89.0 ± 15.4**	0.00030 ± 0.00006	0.031 ± 0.009*	60 ± 26*
4a	245.6 ± 2.9***	295.3 ± 23.9***	0.00007 ± 0.000002***	0.020 ± 0.002***	54 ± 7**
4b	174.6 ± 4.3**	158.5 ± 8.1***	0.00006 ± 0.00001***	0.009 ± 0.001	121 ± 22
5a	185.0 ± 1.6***	125.6 ± 6.2***	0.00011 ± 0.00001***	0.013 ± 0.001**	79 ± 8**
5b	192.1 ± 6.4**	148.7 ± 9.8***	0.00010 ± 0.00002**	0.015 ± 0.003*	82 ± 22*
6	288.9 ± 16.4**	277.1 ± 12.2***	0.00004 ± 0.00001***	0.012 ± 0.002*	87 ± 12*

[a] Values represent means ± SEM derived from two independent experiments for IC_{50} values (Figure S5) and at least 5 for other parameters.

[b] Statistical significance as per Student's *t*-test is indicated.

*, **, and *** represent *p* values of ≤ 0.05; ≤ 0.01, and ≤ 0.001, respectively, for analogues vs. **1**. ●, ●●, and ●●● represent p values of ≤ 0.05; ≤ 0.01, and ≤ 0.001, respectively, for **3a** vs. **3b**, **4a** vs. **4b**, and **5a** vs. **5b** pairs. No dots or asterisks indicate no statistical significance.

Table 2.

Susceptibility of *M. smegmatis* strains to salicyl-AMS

***Msm* strain (EXO / MBT)**[a]	**MIC (μg/ml)**[b]	
	GASTD medium	**GASTD+Fe medium**
Msm WT (+ / +)	>1000	>1000
Msm ΔE (− / +)	0.5 – 1.0	>1000
Msm ΔM (+ / −)	>1000	>1000
Msm ΔEM (− / −)	no growth	>1000
Msm ΔEM-pMbtA$_{tb}$ (− / +)	0.5 – 1.0	>1000

[a]The siderophore production phenotype of each strain is indicated between brackets. EXO, exochelins; MBT, mycobactins; +, production; -, deficiency.

[b]MIC data shown is derived from three independent experiments.

Table 3.

Antimicrobial activity and post-antibiotic effect of $MbtA_{tb}$ inhibitors in *M. smegmatis* **Δ**EM-p$MbtA_{tb}$

Cmpd.	MIC (μg/ml)[a]			PAE (hours)[c]		
	GASTD medium		GASTD+Fe medium	5× MIC	50× MIC	100× MIC
	range	mean				
1	0.5 – 1[b]	0.8 ± 0.2	>64	9.4 ± 1.6	14.2 ± 0.9	34.5 ± 1.8
2	4 – 8	5.3 ± 1.3*[d]	>64	-0.1 ± 0.8**	12.3 ± 3.5	32.7 ± 2.5
3a	1 – 2	1.3 ± 0.3	>64	5.7 ± 2.9	30.3 ± 5.5*	49.9 ± 3.7*
3b	1	1.0 ± 0	>64	14.4 ± 1.9	25.0 ± 1.0**	35.7 ± 2.0
4a	1	1.0 ± 0	>64	10.6 ± 2.7	18.7 ± 1.3	23.1 ± 3.1*
4b	0.5 – 1	0.8 ± 0.2	>64	13.4 ± 2.6	17.4 ± 4.7	19.4 ± 2.2**
5a	2 – 4	2.7 ± 0.7	>64	9.0 ± 0.9	12.2 ± 1.2	32.9 ±6.2
5b	4 – 8	5.3 ± 1.3*	>64	4.0 ± 1.5	23.2 ±2.9*	45.7 ± 3.8
6	4 – 8	5.3 ± 1.3*	>64	18.6 ± 2.8*	ND	ND

[a] MIC data against *Msm* ΔEM-p$MbtA_{tb}$ shown represent ranges and mean values ± SEM of $n = 3$ independent experiments.

[b] The MIC value for **1** was derived from experiments independent from those that rendered the MIC value shown in Table 2.

[c] PAE was calculated as the difference between the time-to-threshold values of the inhibitor-exposed culture and the control cultures (Figure S9). The PAE data in *Msm* ΔEM-p$MbtA_{tb}$ represent mean values ± SEM of $n = 3$ independent experiments.

[d] Statistical significance as per Student's *t*-test is indicated.

*, *, and *** represent p values of ≤0.05; ≤0.01, and ≤0.001, respectively, for analogues vs. **1**. ● represents p value of ≤0.05 for **3a** vs. **3b**, **4a** vs. **4b**, and **5a** vs. **5b** pairs. No dots or asterisks indicate no statistical significance. ND, not determined.